Spring 4-27-2017

Kinematics of the Lower Extremities during Fundamental Martial Arts Tricking Techniques

Kevin P. Grassie
University of Connecticut - Storrs, kpgrassie@gmail.com

Kinematics of the Lower Extremities during Fundamental Martial Arts Tricking Techniques

Kevin Grassie

Honors Thesis
Advisor: Dr. Krystyna Gielo-Perczak
Department of Biomedical Engineering
University of Connecticut

Table of Contents

Acknowledgements

Thank you to the University of Connecticut Department of Biomedical Engineering and Dr. Krystyna Gielo-Perczak especially for access to the biomechanics laboratory, guidance on the many steps of the project, and access to the motion capture system and equipment. Special thanks to the past UConn students who wrote a comprehensive manual on operating the motion capture software.

YouTube Links to Sample Trials of Each Technique:

- Corkscrew: https://www.youtube.com/watch?v=NMo582dV1_I
- Front Snap Kick: https://www.youtube.com/watch?v=DzlPBhPPeZs
- Spinning Hook Kick: https://www.youtube.com/watch?v=93jSZUJ7Kec
- Roundhouse Kick: https://www.youtube.com/watch?v=yJjA5VfdD-Q
- Side-blade Kick: https://www.youtube.com/watch?v=YbKZt5jwsv0
- Tornado Kick: https://www.youtube.com/watch?v=-8YfKuYD1YE

I: Introduction

Orthopedic biomechanics is the study of the mechanical physics of the musculoskeletal system in all aspects of human locomotion. It has wide applications in sports science, conditioning, personal healthcare, and the advancement of medicine. For almost all people, sports and basic physical fitness are important to leading a healthy life. In the process, however, many people need medical attention at some point in their life because of musculoskeletal complications or injuries. Orthopedic biomechanics research aims to better understand how the body moves and functions, and has direct implications on the care and health of many.

Orthopedic biomechanics research generally involves studying three main properties about the musculoskeletal system during activities: loads, kinematics, and muscle activity. Loads are defined as the forces and torques applied to or generated by bones, muscles and joints, when interacting with the world around them. This is typically done with force-torque transducers, which convert external loads into electrical signals to be analyzed by a computer. These transducers can be rigid, externally fixed devices, or implantable, flexible devices – the latter typically done for cadaver specimens.

Kinematics includes the relative linear and angular positions, velocities, and accelerations of different body segments, and how these quantities change in space and time during activities. The standard for recording these quantities is through motion capture systems. Motion capture is a technology that is typically seen in the entertainment industry, but it has significant utility in tracking body segments for biomechanical purposes as well. By tracking the kinematics of infrared markers attached to a subject, linear algebra computations can be done to describe the

kinematics and coordinate systems of anatomical regions of interest (e.g. the motions and loading distributions at the knee during walking).

Muscle activity is the electrical activity associated with muscle fibers, that is directly related to the mechanical activation and force generated by a muscle. By studying these three in tandem, researchers can understand the full picture of what the body is doing during a motion, from voluntary movements, involuntary responses, and reactions from the environment. Muscle activity is generally recorded using electromyography (EMG), where electrodes are placed in the proximity of muscles so that they detect electrical changes across the electrodes that correlate with muscle activation. Many modern EMG systems use wireless, adhesive sensors so that the subject is free to move naturally without being impeded by hardware. The electrical patterns that are recorded from muscles can help researchers see trends on how different people move, as well as diagnose potential muscular complications.

Sports are one of the many important focuses of orthopedic biomechanics research. Being that they are common pastimes for people of all ages in our society, they are enormously relevant in the clinical environment. Sports allow people to stay fit and healthy, but can often also cause injury and long-term health complications if not performed correctly or if accidents happen. Orthopedic biomechanics fits in by applying the laws of mechanical physics to the human body in order to obtain a deeper understanding of different movements and activities in sports. Performing measurements and experiments on human movement, ranging from simple balance while standing to dynamic athletic activities, is crucial for understanding how the body interacts real-time with its environment. The results of such research can be translated into improved therapy, training regiments, technique, and conditioning for athletes and others, to prevent acute or chronic injuries to their bones, muscles, and joints.[15]

From the clinical perspective, orthopedic injuries, either from sport or lacking a certain level of physical fitness, are the most common reasons people need medical care. According to the American Academy of Orthopedic Surgeons, the most common sub-specialty for orthopedic surgery is sports medicine, followed by hand surgery and total joint replacements. On average, seven million Americans are hospitalized for orthopedic complaints or complications, annually.[17] The need is clearly present for continued research and understanding of body mechanics, so that physical therapists, health care providers, and surgeons can understand how to help people recover faster and sustain healthy lives in all that they do.

Among the many sports that have been well known and studied for generations, there are some that have been recently born and on the rise, which need to be better understood. One of these is "Martial Arts Tricking." Martial Arts Tricking – or "Tricking" for short – is a very young movement sport that involves performing aesthetic and stylized combinations of martial arts kicks with gymnastics-style flips and twists. Unlike many other styles of martial arts, the primary goal of the movements is not for self-defense, but rather for self-expression and pushing one's body to the limits of what is possible in acrobatic movement. Tricking derives its movements from traditional arts including but not limited to Taekwondo, Wushu, Capoeira, gymnastics, and breakdancing.[16]

The sport came to be sometime in the 1980s, where martial arts competitors and entertainers began experimenting with moves from different styles, purely out of fun. However, with the rise of the internet and video-sharing websites like YouTube, the sport grew exponentially in popularity through the 1990s and 2000s into a worldwide phenomenon. Tricking today is a global community of athletes from different nations and ethnicities, who share a common love for the highly dynamic and complex individual sport. Tricking has a

culture all of its own, with different athletes having different body types, movement styles, and expression in their tricks.[16]

From a biomechanical standpoint, this young sport offers a plethora of new mechanics to study. While the sport is built from other disciplines that have been around for decades, the fusion of these movements creates something brand new. Tricking differs from its separate influences in that skills often incorporate immediate transfer of non-linear momentum from one trick to the next, off-axis flips and twisting rotations, rapid changes in inertia with kicks during flips, and complicated body positions that require enormous strength and flexibility.

There has been some published research on the biomechanics of martial arts, gymnastics, and basic activity, treated as separate entities. For example, the kinematics of the lower extremities during gait cycles and simple jumping are commonly studied for the purposes of physical therapy and injury prevention for all people.[6,9,18] Regarding martial arts, Jake N. Pearson from the University of Otago, NZ studied the kinematics and kinetics of the Taekwondo roundhouse kick using optical videography and computational methods.[1] Additionally, Kim et. al analyzed how the distance to a target affects the kinematics of the trunk, pelvis, and kicking leg during a roundhouse kick.[11] The work by Sorensen et. al examined the muscular dynamics of the leg during a front kick to the face, using electromyography and high speed cameras to capture muscular activity during the deceleration of the kick at the point of impact.[3] From the perspective of mechanical modeling vs. experiment, Maria Roy Felix et. al conducted broad calculations regarding the mathematics of different karate techniques.[5]

Examples of gymnastics research only include the study of traditional, linear movements. Mkaouer et. al studied the kinematics of different tumbling series leading up to a backward layout somersault, with motion capture and force platform recordings.[7] Meanwhile, the kinetics

and muscle activity of gymnastics transitions and takeoffs, such as the back handspring have been studied as well.[8,13] Broader analyses have been done about the prevalence of injuries in gymnastics, such as the research conducted by Bradshaw et. al.[12]

Potential refinements of biomechanical investigation procedures have also been published, in research such as that conducted by Borhani et. al and Yahia-Cherif et. al. These authors focused on revising motion capture marker setups and visualization of the pelvis and hip for optimal kinematic analysis.[14,19] Taking these examples into consideration, the consensus from the literature review performed by Mustapha et. al, focused on surveying known publications about martial arts biomechanics, is that more investigations need to be done.[4]

Nevertheless, there is almost no literature on the sport of Tricking specifically, where the techniques and movements are quite unique from anything seen in traditional martial arts and gymnastics. Moreover, with the growing sensation of the sport worldwide, more young people are getting involved at local gyms and in their backyards, often without a formal training structure in place. As a result, the incidence of Tricking injuries has risen due to poor conditioning, higher participating population, and/or accidents. The lack of literature makes it difficult to understand the mechanisms of these injuries and how to avoid them, so that athletes can make the most of the sport. This is primarily because the mechanisms of the tricks themselves are still mostly unknown. Thus, there is a great need for biomechanical research to explore the sport of Tricking and those who participate in it, because it has clinical relevance and involves new types of motion not previously studied.

The purpose of this study is to conduct a preliminary biomechanical analysis of Martial Arts Tricking. Kinematic observation and analysis via motion capture were performed on a single subject performing four basic kicking techniques and two dynamic tricks involved in

Tricking. in order to propose and test a framework for analyzing such complex, dynamic techniques. Additionally, many of the techniques were conducted on both sides, so that comparisons and evaluations of bias could be made between mirror images of the techniques. The motivation for this study is in reference to the work from Perez et. al, where kinematic differences between standing and jumping kicks were studied using motion capture.[2] This study aims to quantify in detail the time-dependent linear velocities and accelerations of the lower extremities during Tricking techniques that have not been analyzed in depth.

II: Methods and Materials

Motion Capture System

The motion capture system used throughout the following experiments was the OptiTrack Motion Capture Suite, owned by the University of Connecticut Biomedical Engineering Department. All of the following technical information about hardware and software is courtesy of OptiTrack.com and the University of Connecticut Operator's Manual for the OptiTrack system by Chomack et. al.[10,20] The main hardware in the OptiTrack system is as follows:

(a) (b) (c)

Fig 1. (a) Flex13 OptiTrack Camera (1 of 6); (b) USB A to Mini USB B Cable: 16' (1 of 6); (c) One Stage Stand Tripod (1 of 6) with tri-axial camera mounts.[10]

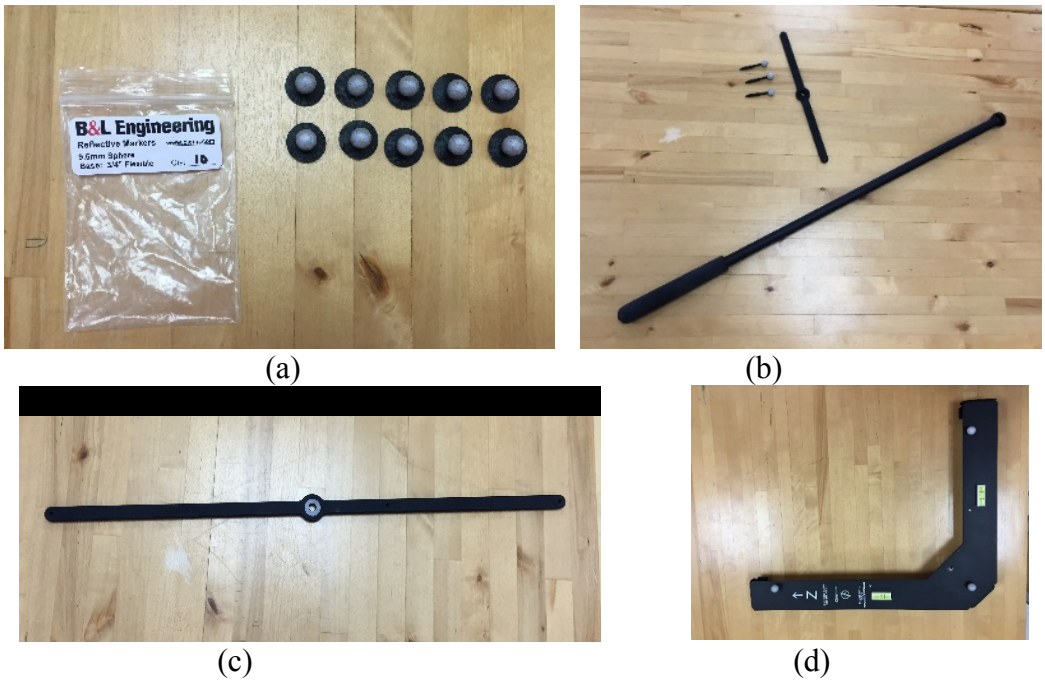

Fig 2. (a) 9.5 mm diameter reflective markers, (b-c) calibration T-wand handle and 500 mm attachment, with three reflective markers attached, (d) calibration L-frame with three reflective markers attached.[10]

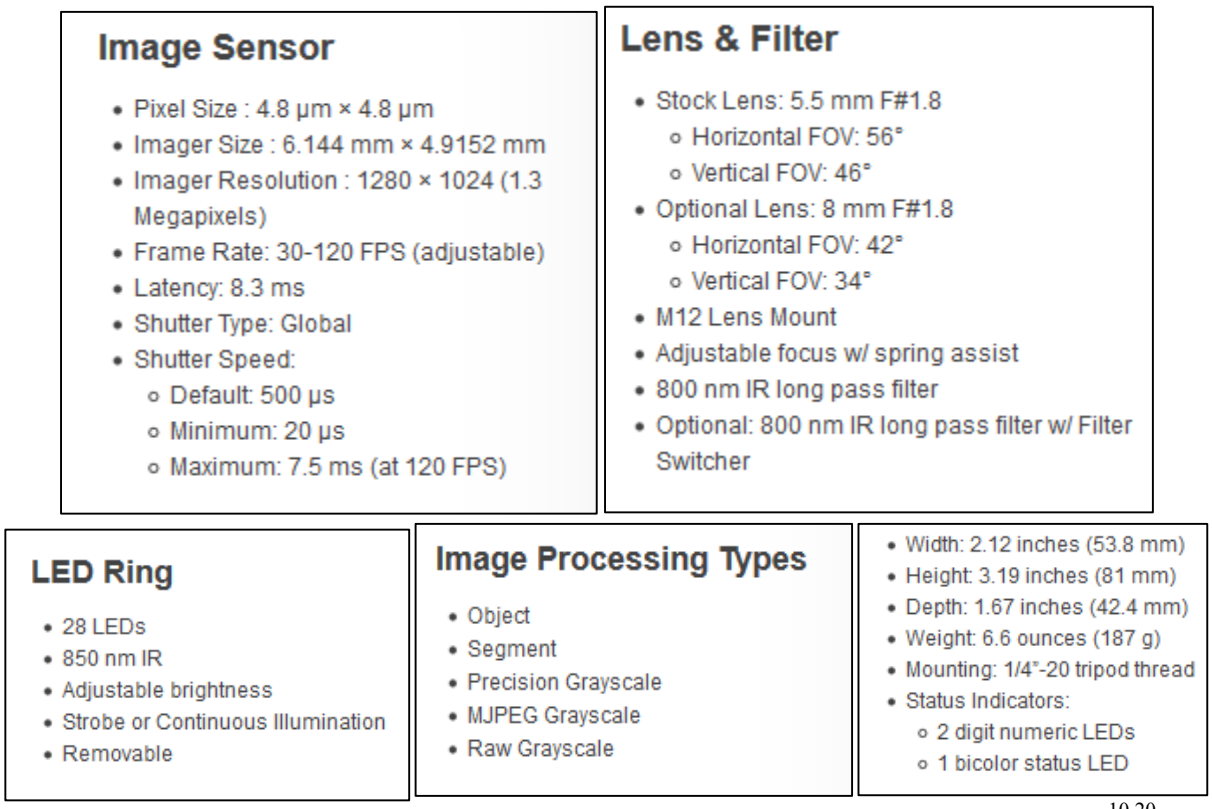

Fig 3. Hardware dimensions and specifications for the OptiTrack Flex13 cameras.[10,20]

(a) (b) (c) (d) (e)

Fig 4. (a) OptiHub box where up to six cameras can be connected via USB, (b) USB activation key for Motive software associated with OptiTrack cameras, (c) USB activation key for Motion Monitor software, (d-e) USB A to B cord and extension for data transfer from OptiHub to computer. (standard AC power cord for OptiHub box not shown)[10]

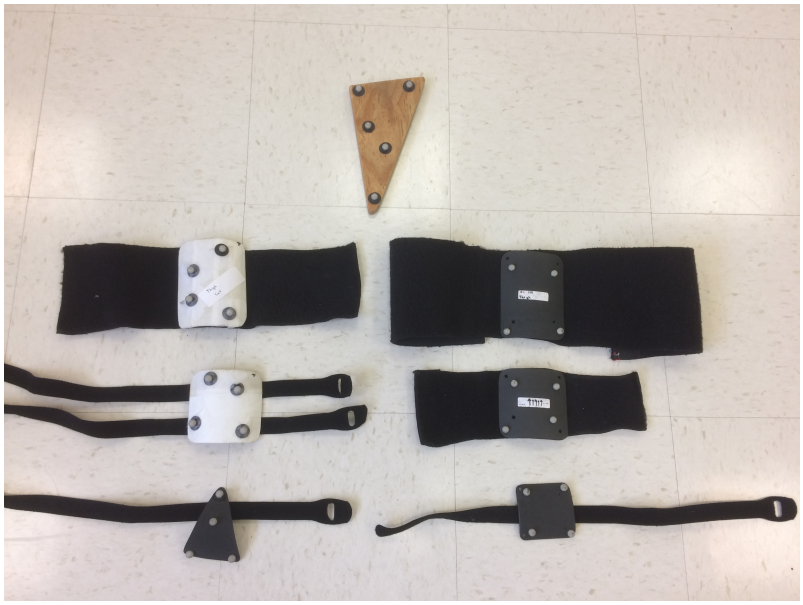

Fig 5. Rigid-body reflective marker groupings for each of the six main bone segments for both legs (thigh, shank, foot x2 – top to bottom). The wooden stylus above is for digitizing within the software. Velcro bands/straps were attached to the rigid bodies to secure them to the wearer.

Capture and Analysis Software

Motive: Tracker (from OptiTrack): The primary capture software for the OptiTrack Flex13 infrared cameras is Motive: Tracker. The software is capable of multiple-camera calibration for up to 24 USB cameras and tracking of up to 2,000 markers with a 3D reconstructed view for the user. The software can implement camera synchronization, rigid body groupings, and multiple smoothing and filtering functions. Motive: Tracker allows many camera parameters to be adjusted, such as blocking visible IR artifacts in view, frame rate, contrast and intensity

threshold, and more. Exported motion data is available in .C3D and .CSV files using the Motive: Tracker system. Additionally, motion data can be streamed to other analysis software packages, as well as triggered to record in synchronization with external sensors (e.g. force platforms, electromyography, etc.). The Motive: Tracker system is very versatile and capable of recording reliable motion data for the experiments conducted in this study.[10,20]

Fig 6. Motive: Tracker software logo and basic user interface

Motion Monitor (version 9): This software is the workhorse of data compilation, interpretation, and analysis from the Motive: Tracker software. First, the Motion Monitor allows for streamed Motive: Tracker marker data to be digitized to correspond to bone and joint motions. The

motions of markers, rigid bodies, and corresponding digitized skeletal segments are tracked and recorded relative to calibrated world axes within the Motion Monitor software. The body segments and world axes are digitized using the calibration L-frame, stylus, and subject-specific rigid bodies seen in Figs. 2 and 5. They are represented in 3D in real-time and recorded animations after setup is complete. Second, the Motion Monitor has the potential to record multiple channels of complicated data from A/D converter boxes simultaneously, while recording motion data. For example, EMG signals and force/torque sensor data can be paired with the streamed kinematics data from Motive: Tracker. From these raw data, position and biomechanical data about each digitized marker, bone segment and joint can be exported as .C3D, .PTB, or .CSV files for further analysis.[10,20]

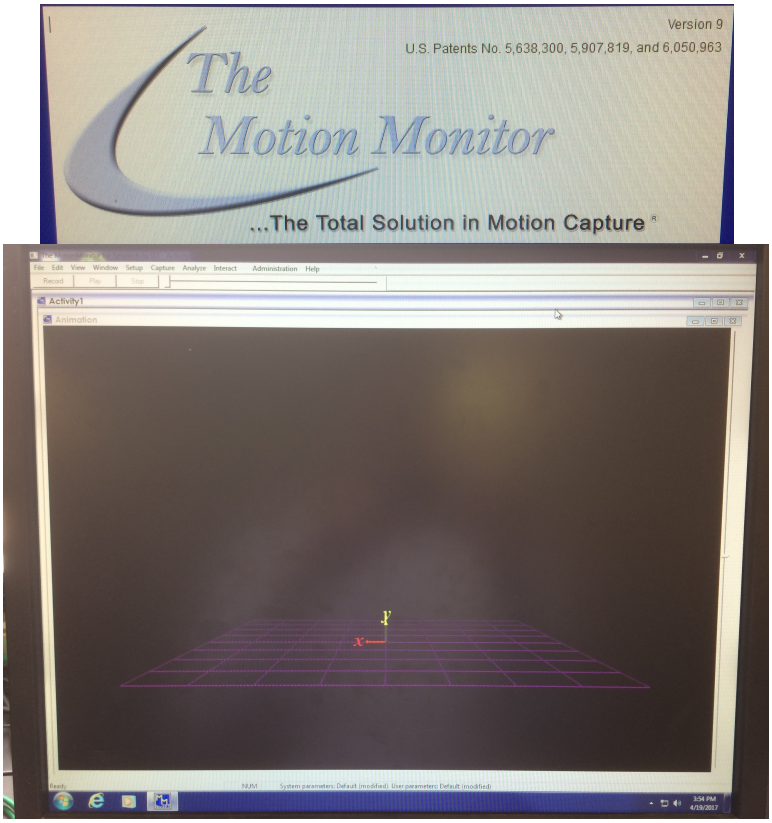

Fig 7. Motion Monitor software logo and basic user interface with the 3D animation view shown; this is where the skeletal movements would be projected after recording a capture.

Further Analysis: Once .CSV files were acquired from the Motion Monitor throughout this study, MATLAB (2013a Student version) and Microsoft Excel (2016) were used to process, organize, plot, and summarize the motion data. Additionally, a GoPro Hero3+ was used to record optical video of the different experimental motion trials, while the free screen recording software IceCream (version 4.75) was used to save the recorded 3D animations from Motion Monitor for each trial. QuickTime Player (2016) was used to manually synchronize the optical and animated videos of the trials. Operating systems used in this study were Windows 7 Enterprise (2009) and Mac OS X El Capitan (version 10.11.6).

Miscellaneous Equipment:

- Metric ruler
- 24 Foam Floor Mats – (Greatmats.com)
    - 2’ x 2’ x 5/8” thickness
    - Interlocking/ “puzzle” mats
- Non-slip rug pads - (Bed Bath and Beyond)
- GoPro Hero3+ (with stand and export cable)

Physical Setup

Successful motion capture is highly dependent on the camera configuration and capture volume. The goal is to ensure that accidental marker disappearances are minimized during captures, by having the cameras’ fields of view overlap and span the appropriate volume of space in which the subject occupies. For dynamic, multi-directional movements such as those found in Tricking, a hexagonal ring was the optimal configuration, given the six cameras and tripods

available to this study. Prior to the camera arrangement, twenty-five interlocking foam mats (2’ x 2’ x 5/8”) were laid down in a 5x5 (10’ x 10’) square. The cameras were then placed roughly 1-2 feet outside the boundary of the mats in a hexagon pattern, so that all wiring would be either on the periphery or not on the mats at all. Some wires were fed underneath the puzzle mats so that they could reach their respective cameras. Additionally, six, non-slip rug pads were placed under the puzzle mats in corners and the center, for two reasons: 1) to keep the mats from slipping on the linoleum floor during different motions and landings, and 2) to elevate the mats slightly and take the stress off of the few wires underneath, while the subject is moving on top of them. The resulting hexagon of cameras had an approximate radius of 6’ (~ 2 m) from the center of the foam mat square.

Each camera was mounted on the One Stage Stand tripods, and elevated to approximately 6-7 feet. The cameras were angled appropriately so that they were facing the direct center of the capture space, where the center tile could be visible in the bottom quarter of each camera’s field of view. This was done so that the cameras could reliably track the markers of the legs and feet when they were low, during standing, and when they were high, during jumps or inversions of the body. All camera USB A-to-Mini-B cords were then fed to the OptiHub box, located at the front of the foam mats (defined as the –Z direction). An AC power cable was connected to a power strip and into the OptiHub, while a USB A-to-B cable connected the OptiHub box directly to a computer USB port. Also at the computer end, the two USB activation keys for the Motive: Tracker and Motion Monitor programs were inserted. A schematic of the entire setup is shown in Fig 8. Note that red and blue mats were arranged as shown to protect the subject and the equipment; approaching blue mats during a technique would serve as a warning to the subject to watch his/her spacing.

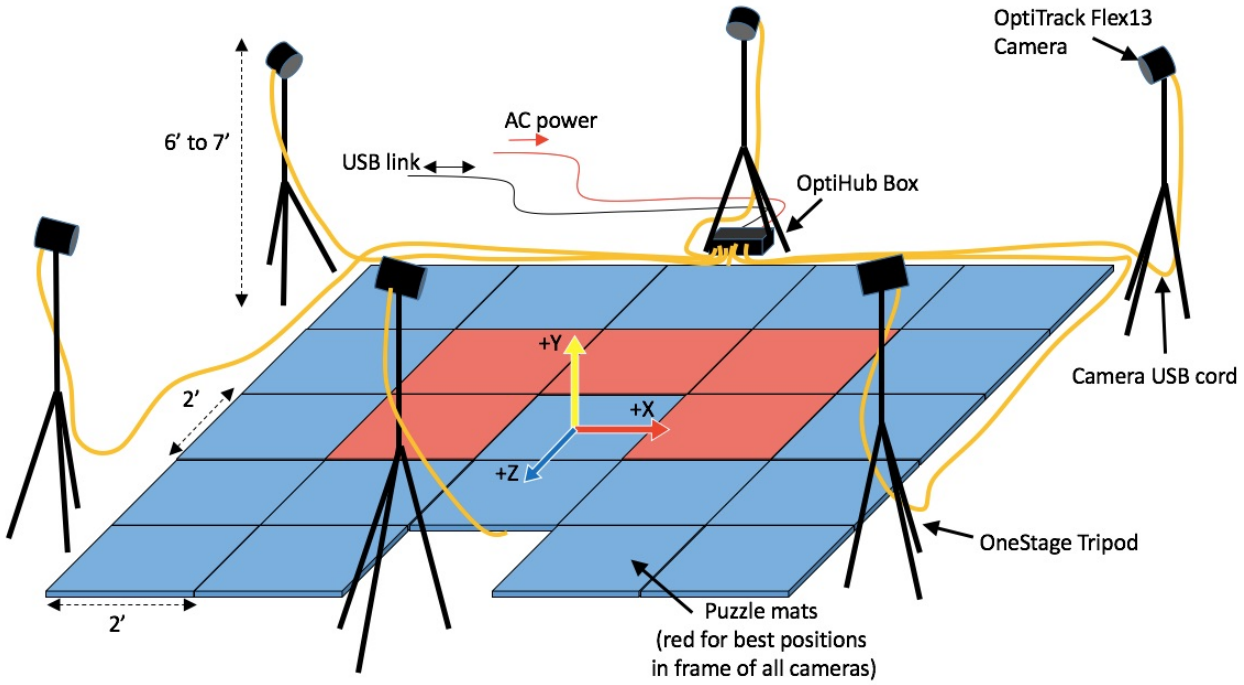

Fig 8. Diagram of capture volume setup, with cameras, foam mats, and wiring shown. The global coordinate axes used by Motion Monitor are shown as well, in the center. (Computer not shown; assumed off in the distance and connected to USB link)

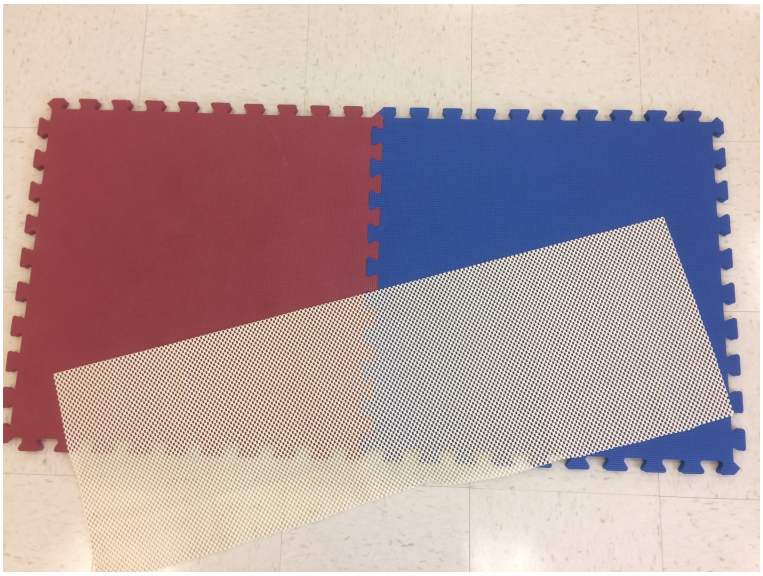

Fig 9. A close-up view of the actual foam mats used, with one of the non-slip rug pads draped over top.

Camera, Capture Volume, and Subject Calibration

* The following procedures for setup and calibration are courtesy of the student-written operator's manual for the Motive and Motion Monitor systems, from the University of Connecticut Department of Biomedical Engineering.[10]

1. Motive: Tracker Program Startup: Once the Motive software was opened, settings for adjusted for timely delivery of synchronized camera data, point cloud reconstruction within the 3D view, and no 2D filter type for the cameras themselves. The cameras were set at their maximum framerate of 120 fps, while having standard settings for contrast, threshold, brightness, etc.
2. Aiming the Cameras: To calibrate the cameras in their configuration, a three-step procedure was used. The first was to aim the cameras properly. The calibration L-frame was placed on the center foam tile such that the axes correspond to those shown in Fig 8. Fig 2d shows the L-frame, where the long arm labeled "z" corresponds to the –Z direction, the short arm corresponds to the +X direction, and the +Y direction comes up from the floor. Once the frame was in place, all six cameras were manually angled on their mounts more precisely so that each could see the three markers of the frame in the central, bottom quarter of their field of view. Then, the L-frame was removed from the cameras' view, and the "Block Visible" option was selected in Motive, to eliminate any camera pixels that show extraneous artifacts, due to metal, surroundings in the room, or reflections off of the floor.
3. Wanding Calibration: Next, the calibration T-wand with 500 mm marker attachment was assembled. In the calibration pane of Motive, "Start Wanding" was selected, and the wand was manually waved dynamically and randomly throughout the entire capture volume, so that all of the cameras could track many samples of the wand's position. 1200

samples per camera was decided upon as an adequate amount to practically minimize tracking and calibration errors. Once 1200 samples were capture, Motive was directed to calculate the calibration, where the software would trace every sample of the wand motion and link the cameras in space based on all 1200 samples. The calculated calibration results were applied once all cameras' statuses read "Exceptional Quality." The mean 3D error for successful calibrations was on the order of 0.1-0.2 mm. The calibration file was then saved.

4. Ground Plane Identification: At this point, the 3D view showed all six cameras in their hexagonal ring, but not oriented so that the floor is parallel with the plane of the hexagon. Therefore, the L-frame was placed back onto the central foam tile, with the same orientation as before. The three markers of the frame were selected in the 3D view of Motive, and "Set Ground Plane" was selected from the Ground Plane window. The final calibration file was saved; two calibration files exist for an entire calibration procedure. The 3D view updated to show all six cameras in their proper positions and orientations, as reflected by Fig 8, where the grid plane corresponds with the foam mat surface.
5. Rigid Body Creation: The next part of the procedure was to create rigid body groupings within Motive, based on the seven marker groupings in Fig 5. The groups were placed as seen in Fig 5 onto the foam mats in the capture space. Due to the proper calibration, the groupings were visibly tracked and easily identifiable in the 3D view of Motive. By highlighting each group and clicking "Create from Selection" in the Rigid Body panel, each group could be created and named. The order of creation for the rigid bodies was Left Thigh, Left Shank, Left Foot, Stylus, Right Thigh, Right Shank, and Right Foot. All but the stylus had 4 markers on them, arranged in distinct quadrilateral polygons so that

Motive would not confuse them. The stylus had 5 markers, with one at the tip of the wooden triangle, for accurate digitization later.

6. Broadcast Data into Motion Monitor: After all rigid bodies were created, the Streaming Pane icon was selected in Motive. “Broadcast Frame Data” was selected, with Local Interface in Network Interface Selection set as “Local Loopback.” At this point, the Motive software could be set aside or minimized, as its role was complete.
7. Motion Monitor Settings: The Motion Monitor software was then opened and default user settings were employed. Under “Data to Collect,” only position/orientation sensor data was checked. Next was to edit sensor assignments; this menu allowed for editing the sensor numbers so that their numerical order matches the order in which the rigid bodies were created in Motive. Under “Administration” parameters, the client and server IP addresses were set for local loopback (127.0.0.1), and the number of markers (29 total), sensors (7 rigid bodies), and framerate (120 fps) were specified. Marker mappings and virtual sensor assignments then appeared, where they were adjusted as necessary to reflect the assignments and chronological order used in Motive.
8. Setting Up Sensors and Space: First, the virtual sensors (rigid bodies) were set up in Motion Monitor. The rigid bodies, now secured at the correct placements on the subject’s body, were placed in the capture space along with the stylus. All rigid body sensors had to be as stationary as possible for the software to register them with minimal error. Second, the stylus was set up. An assistant without any reflective markers on their person sat in the capture space with the stylus, so that only the stylus markers could be observed. To set up the stylus, 10 capture samples were taken where the stylus tip was fixed on the foam mats, and the rest was free to rotate into unique orientations. Once complete, only

small errors (~0.1-1 mm) were present for the stylus registration. Third, the global virtual axes of the capture space were defined. The assistant placed the L-frame back into frame, in the same orientation as discussed earlier. The stylus was first recognized in the software, and then used to mark key points along the L-frame, to define the axes. The origin, being the corner marker of the L, was defined first, by placing the stylus tip directly on the marker. Then, the metric ruler was used to register a point 20 cm in the +X direction still in the plane of the L-frame. The vector between origin and here defined the +X axis. The ruler was then used to register a point 20 cm in the +Z direction, still in the plane of the L-frame. The vector between origin and here defined the +Z axis. Finally, the stylus was held anywhere above the ground plane to define "up" as the direction of the +Y axis. With the world axes established, the last step was to digitize the human body of the subject performing the movements.

9. Digitization of Relevant Skeletal Joints and Segments on the Subject: Under "Setup Subject Sensors," digitization was chosen as the method of setup. The approximate mass and height of the subject were entered while all other settings were kept standard. Two assistants were required for this step: one at the computer, and one holding the stylus and digitizing the subject. The subject and all rigid body sensors except the stylus had to remain very still, and in the anatomical position. The Motion Monitor software runs a procedure where the stylus tip is to be placed at each joint for 10 samples, for a sequence of all relevant joints. In this case, the sequence was left hip, left knee, left ankle, left foot 2nd phalanx, right hip, right knee, right ankle, and right foot 2nd phalanx. Four anatomical points were chosen on each leg so that three body segments could be proportionally and

properly attributed to the rigid body markers' movements. After digitization, an assembled, lower extremity skeleton could be seen in the 3D view of Motion Monitor.

10. Running a Test Capture to Adjust Data to Analyze: Under "Capture," a test recording was conducted via "Record Activity." Then, under "Analyze", "Real-time", in the Segments tab, the desired time-dependent mechanical and dynamical data could be selected, in vector or magnitude form.
11. Running a Capture and Exporting Data: Closing out of the digitization window, and adjusting recording parameters, such as length of time of capture, an assistant could record the subject's activity. The activities were then saved locally to the computer and could be re-opened for analysis at any time. The data vs. time for a given activity could be exported as a .PTB file, which is compatible with Microsoft Excel. The Excel files were then saved and prepared for MATLAB analysis and plotting.

Capture Video Presentation and Analysis Procedure

During recordings of different Tricking techniques, a GoPro Hero3+ camera was used to record the activities in visible wavelengths of light. The footage from the GoPro was used to keep track of how the entire subject's body was moving and what the trick actually looks like, since Motive and Motion Monitor only track the lower extremities and their markers. To save the animations of each captured technique from Motion Monitor, a free screen recording software called IceCream was used while playing back the animations.

Two copies were made of the saved animations. One was trimmed so that time 0:00 in the video corresponded with time 0:00 in the animation itself. This version would be important for understanding what the subject was doing in real life at the same time-stamps as seen in the

Excel/MATLAB data. The other copy of the animation video was trimmed so that it was synchronized with the beginning of the GoPro video of the performed techniques. The synchronization was performed by eye with the Trim feature in QuickTime Player on Mac OS X. The uncertainty in this synchronization procedure was estimated as a 0.05-0.1 s difference between videos. This version of the animation was used for the visuals shown later in the results.

For the analysis, the .PTB data files for a given recorded activity were converted into Excel files and read into a MATLAB script as a large data matrix. Then, plots against time were made for each recorded mechanical quantity. Comparing the plots with the 3D Motion Monitor animations allowed for any data spikes or anomalies to be removed, based on glitches in the animation. These glitches were often due to a) one or more of the subject's body segments and reflective markers moving outside of the capture volume, or b) markers being obscured from the cameras based on awkward body positioning during the techniques. After obvious anomalies were removed, a digital low-pass filter and a moving-average smoothing process were employed in MATLAB. The low-pass filter had an order of 400 and a cutoff frequency of roughly 20 Hz, to eliminate any high-frequency noise due to motion capture glitches. The smoothing process took a moving average of 10 data points across each vector in the data matrix. These values were chosen to give an optimal compromise between smoother data and loss of higher frequency information, which is inherently involved in techniques as dynamic and powerful as those in Tricking. Final plots were made for each trial of each technique performed by the subject.

Experimental Design

Table I: Tricking techniques captured and analyzed in this study. The first four techniques are fundamental martial arts kicks with minor modifications that are performed frequently in Tricking. The second to last technique is an example of a more dynamic, jumping kick. The final technique is an example of an advanced dynamic trick involving body inversion. Because of the difficulty and limitations on laboratory space, this technique was captured only once, from one side.

Technique	Description	Both Sides?	Trials Per Side
Front Snap Kick	Chambered forward-striking kick to the chest, with the ball of the foot	Yes	$n = 4$
Side Kick	Chambered side-striking kick to the head, with a pivoting stance, kicking with the foot's outside edge	Yes	$n = 4$
Roundhouse (Round) Kick	Chambered forward-striking kick to the head with a hip turnover and pivoting stance, striking with the top of the foot across the head	Yes	$n = 4$
Spinning Hook Kick	Chambered forward-striking kick to the head with a full 360˚ pivoting stance and hip turnover, striking with the heel of the foot across the head	Yes	$n = 4$
Tornado Kick	Cheated 360˚ jumping roundhouse kick. The first 180˚ is a stance change on the ground leading to a one-legged takeoff. The second 180˚ is a hip turnover that gives momentum to the airborne round kick	Yes	$n = 4$
Corkscrew	Back flip with a full twist along the longitudinal axis, while swinging off of and landing on one leg	No (CW twisting side only)	$n = 1$

Table II: List of kinematic quantities recorded and exported from the Motion Monitor software for each trial of each technique in Table I. Plot figures of these quantities vs. time were saved for each trial. (COM = body segment center of mass)

Body Segment	COM Linear Velocities	COM Linear Accelerations
Left Thigh	X, Y, Z, Mag.	X, Y, Z, Mag.
Right Thigh	X, Y, Z, Mag.	X, Y, Z, Mag.
Left Shank	X, Y, Z, Mag.	X, Y, Z, Mag.
Right Shank	X, Y, Z, Mag.	X, Y, Z, Mag.
Left Foot	X, Y, Z, Mag.	X, Y, Z, Mag.
Right Foot	X, Y, Z, Mag.	X, Y, Z, Mag.

After all figures were plotted and saved for each trial of each technique tested, the maximum absolute value of each quantity (x-y-z velocity, velocity magnitude, x-y-z acceleration, and acceleration magnitude) for each body segment (see Table II) during each trial was recorded and organized into an Excel summary file. For each technique, the average and standard error for the maxima for each quantity were calculated, for contralateral sides of the techniques. As an example, the Tornado kick had 4 trials on left side and right side. For each trial, maximum magnitudes for x-y-z velocity, x-y-z acceleration, velocity magnitude, and acceleration magnitude of the left thigh, right thigh, left shank, right shank, left foot, and right foot were recorded. For each of these 8 quantities for 6 body segments, separate average and standard error value over four trials were found for each kicking side. These were organized into bar graphs based the kicking direction, kinematic quantity, and technique under investigation.

Subject Information

Age	**Sex**	**Height (m)**	**Mass (kg)**	**Martial Arts Experience (yrs)**	**Martial Arts *Tricking* Experience (yrs)**	**Injuries?**
21	Male	1.78	65.9	15	5	Left Hamstring Tear (2015)

Warm-Up/Recovery for Subject

The subject performed roughly 5-10 minutes of dynamic and static stretching prior to performing the recorded techniques. Warm-up techniques included quadriceps and hamstring static stretching, dynamic leg swings, ankle rolls, gluteal stretches, split stretches, core twists, neck rolls, and shoulder stretches. Between trial sets of a given technique, the subject was allowed to rest for 1-2 minutes, to avoid muscular fatigue and risk of injury.

Assumptions and Limitations

- Only one subject's techniques were tested at the moment, to prove the concept of this study's analysis.
    - More subjects of different body types, skill level, and fitness should be tested in the future to obtain more global results regarding Tricking as a whole.

- The order of trials and techniques performed was random, but consistent.
    - To remove any potential bias in the order of performance, the order of trials and techniques should be randomized and be *inconsistent* between participants

- All trials were conducted on the same day, in the same one-hour window of time.
    - In the future, many more trials of each technique, over the span of many recording sessions, could provide a representative average of a participant's skill level, energy, and performance during the various techniques.

- The techniques chosen were representative of the three basic tenants of Tricking: kicking, flipping, and twisting.
    - More techniques of all three tenants could be tested going forward, so that a more comprehensive view of Tricking is analyzed.

- It is assumed that the errors in motion capture were sufficiently minimized during manual anomaly removal, low-pass filtering, and moving-average smoothing

III: Results

Front Snap Kick

(a)

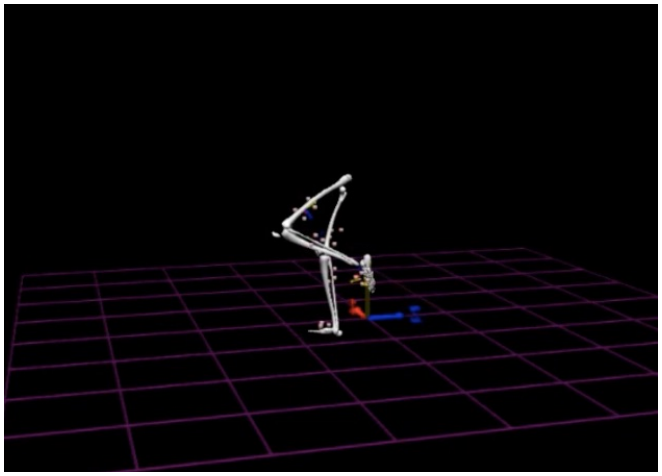

(e)

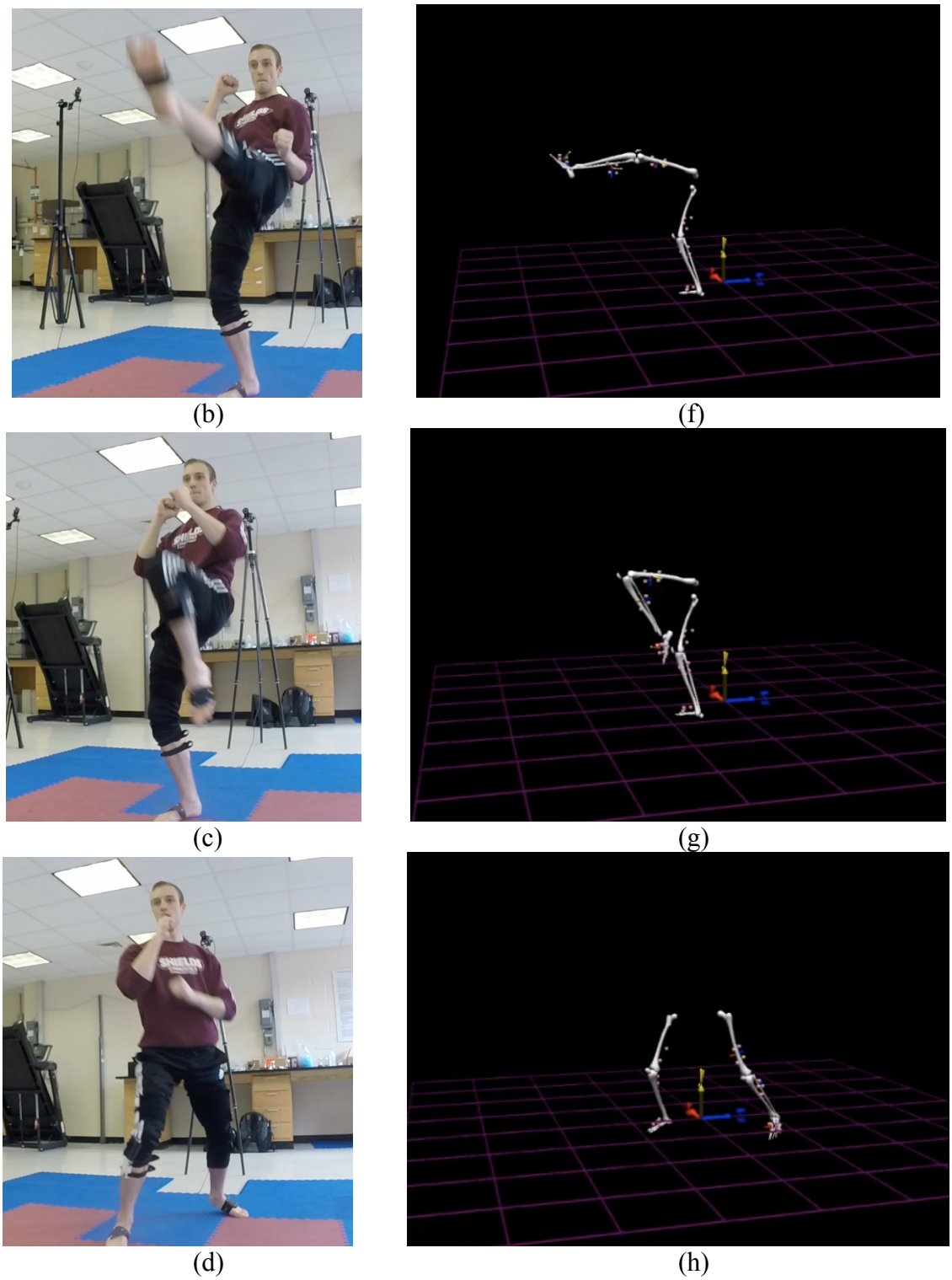

(b) (f) (c) (g) (d) (h)

Fig 10. GoPro video screenshots (a-d) and corresponding synchronized animation frames from the 3D view from Motion Monitor (e-h), for a representative *front snap kick* (here, with the left leg)

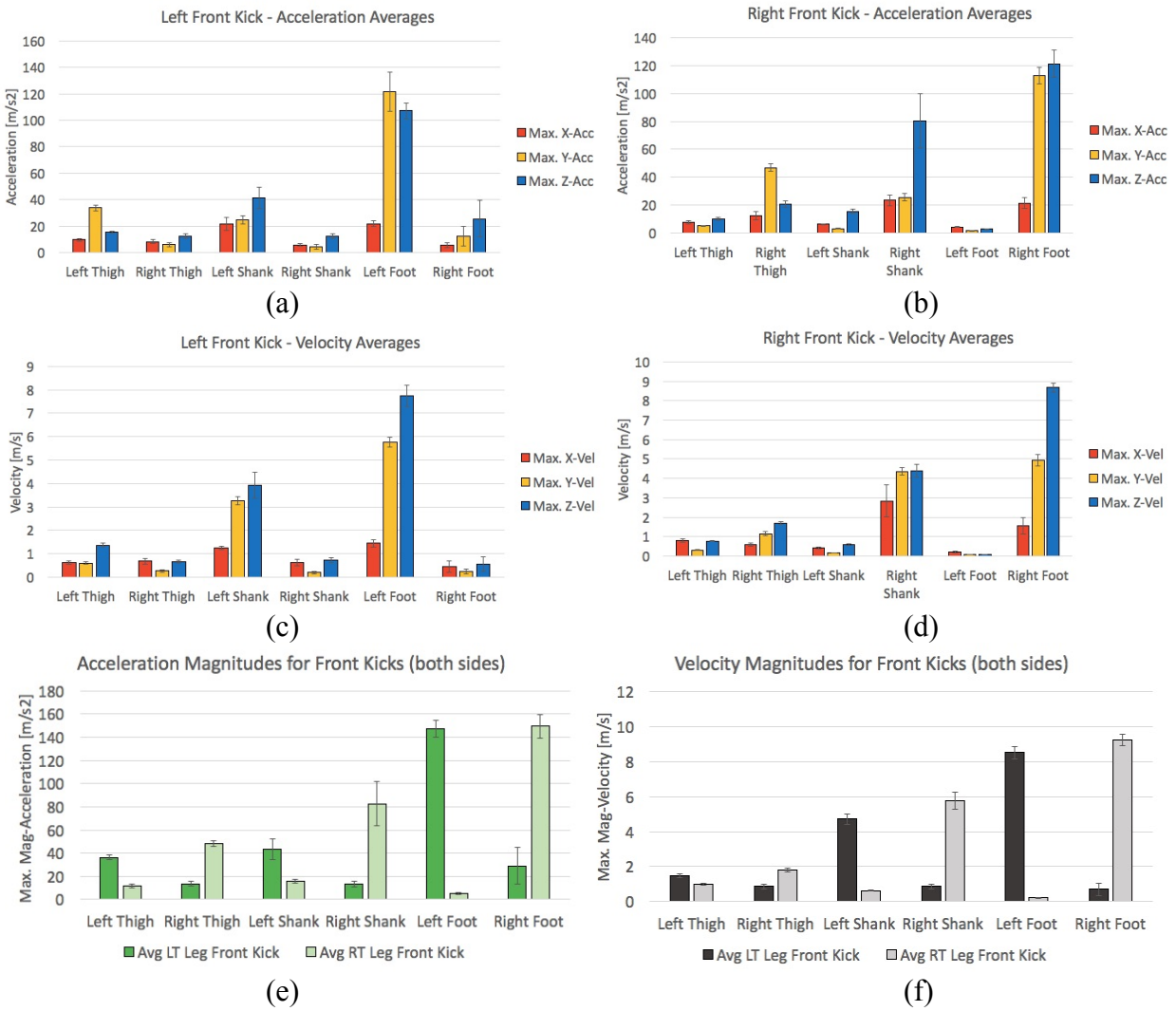

Fig 11. Summary bar graphs for maxima of x, y, z, and magnitude components of linear acceleration and velocity, averaged over all four trials of right-side and left-side *front snap kicks*. Error bars represent standard errors (n = 4).

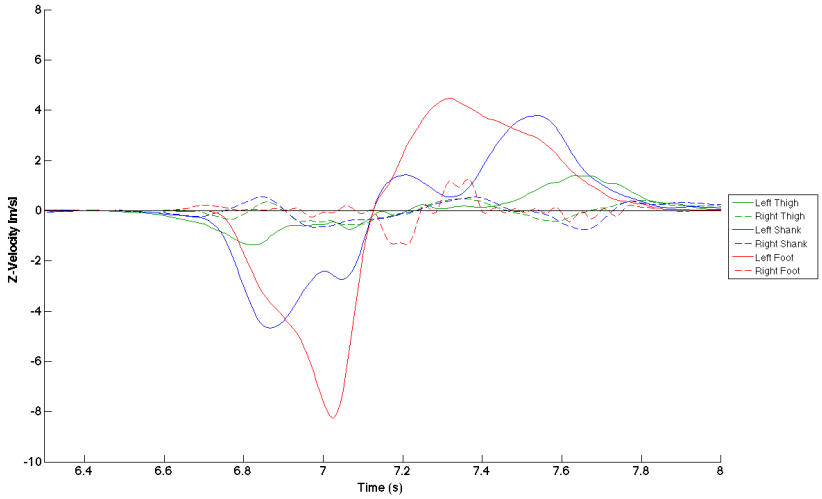

Fig 12. Example plot of the z-component of velocity vs. time for all segments, during a left-side front snap kick. The movement pattern here is representative of all trials of this technique.

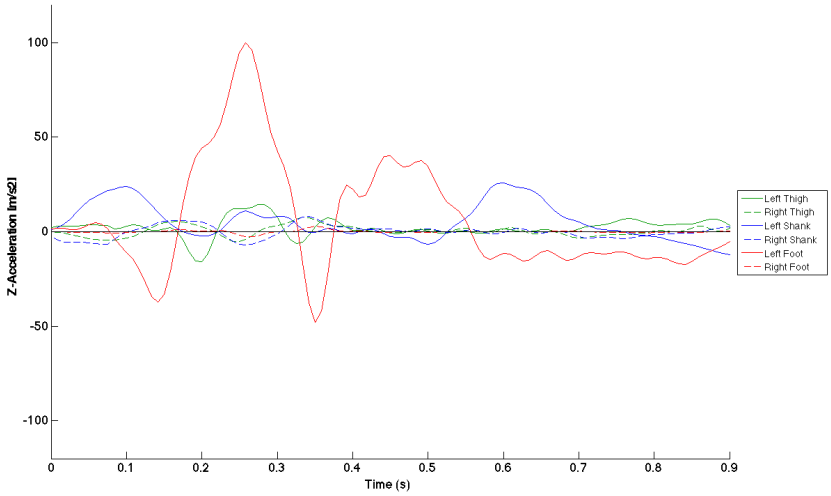

Fig 13. Example plot of the z-component of acceleration vs. time for all segments, during a left-side front snap kick. The movement pattern here is representative of all trials of this technique.

Side Kick

(a)

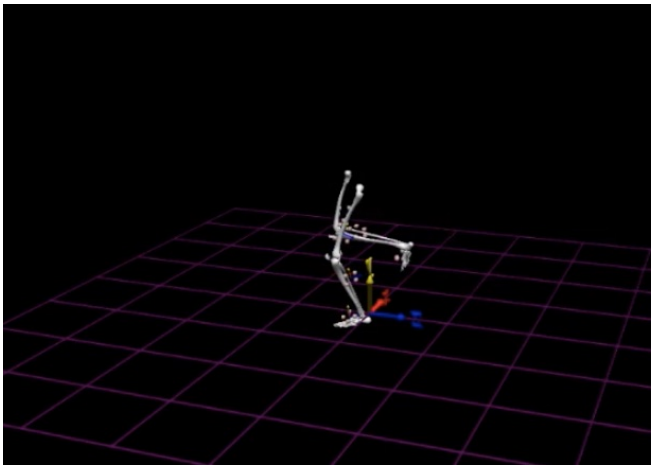

(f)

(b)

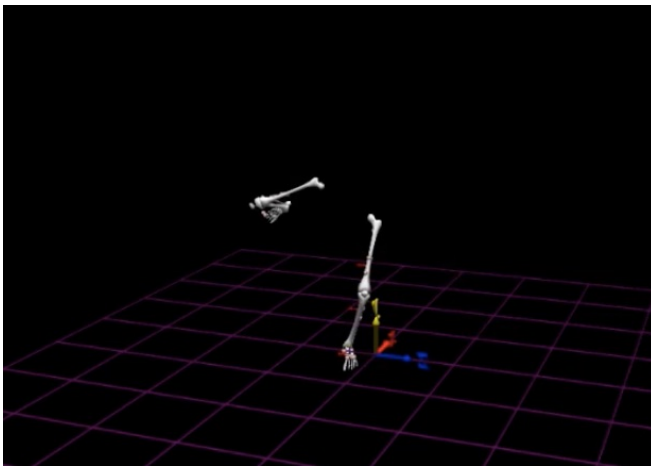

(g)

(c)

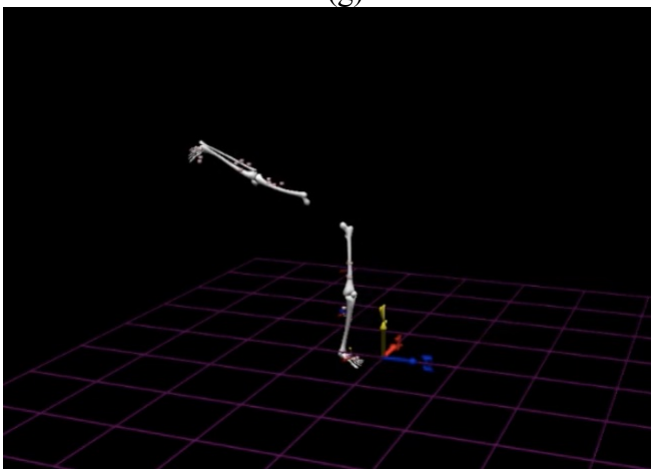

(h)

(d)

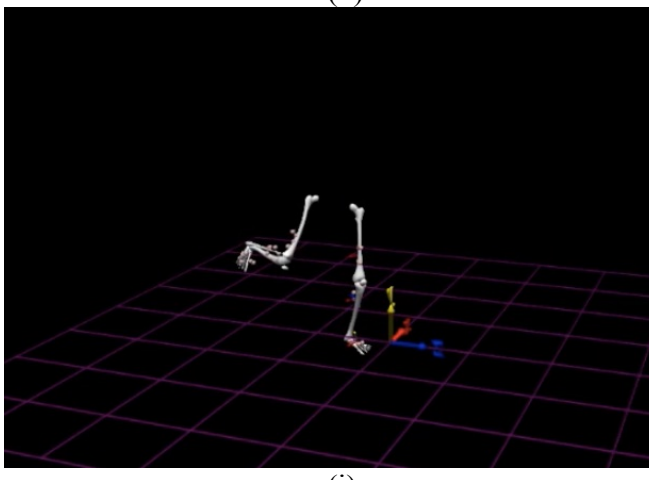

(i)

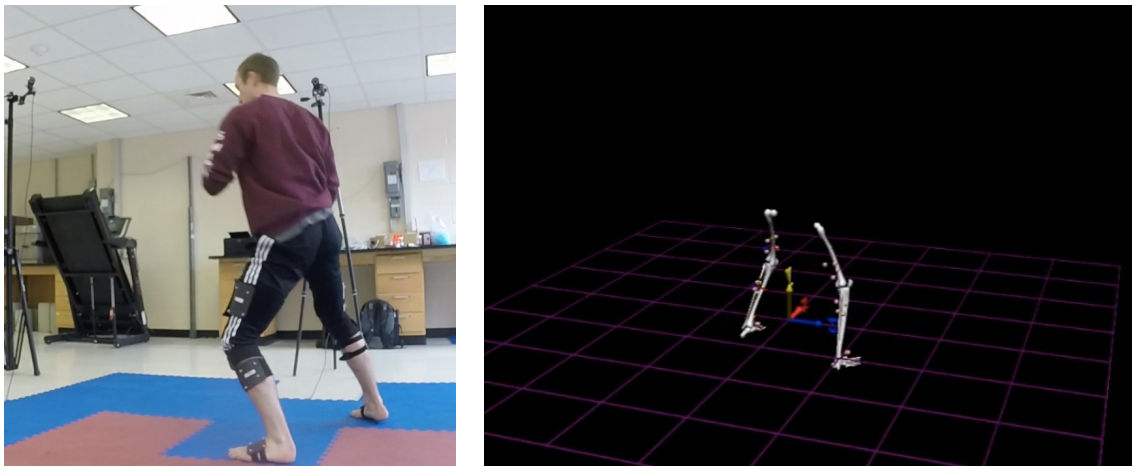

(e) (j)

Fig 14. GoPro video screenshots (a-e) and corresponding synchronized animation frames from the 3D view from Motion Monitor (f-j), for a representative *side kick* (here, with the right leg)

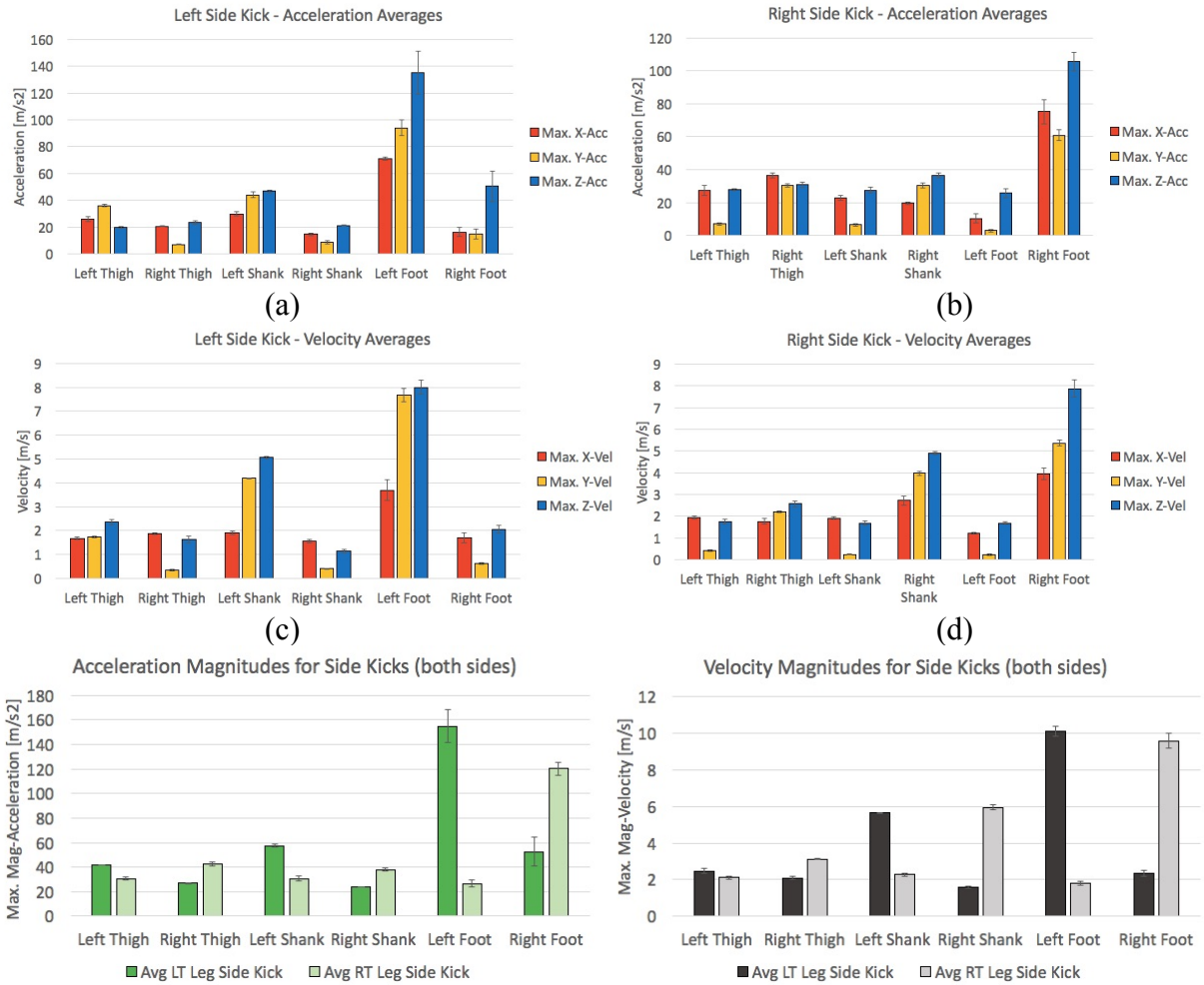

Fig 15. Summary bar graphs for maxima of x, y, z, and magnitude components of linear acceleration and velocity, averaged over all four trials of right-side and left-side *side kicks*. Error bars represent standard errors (n = 4).

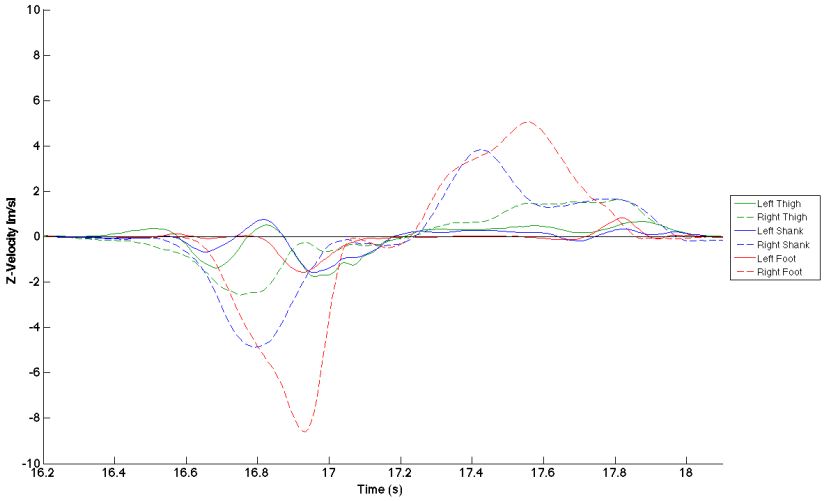

Fig 16. Example plot of the z-component of velocity vs. time for all segments, during a right-leg side kick. The movement pattern here is representative of all trials of this technique.

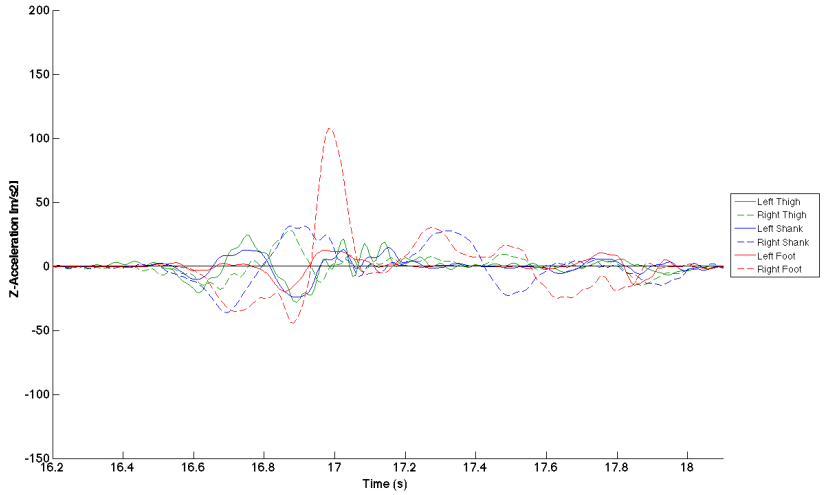

Fig 17. Example plot of the z-component of acceleration vs. time for all segments, during a right-leg side kick. The movement pattern here is representative of all trials of this technique.

Roundhouse (Round) Kick

(a)

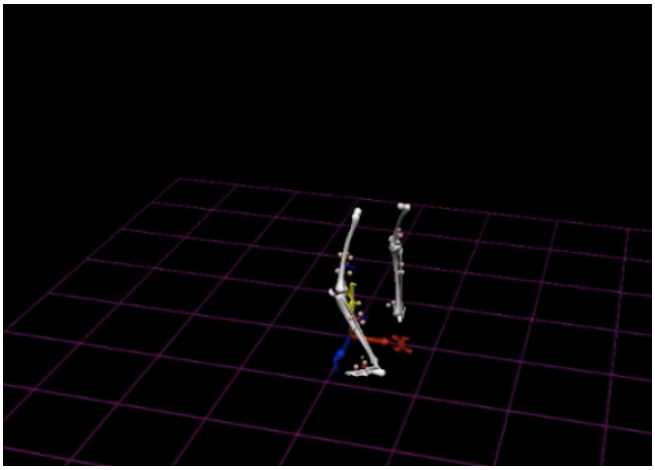

(h)

(b)

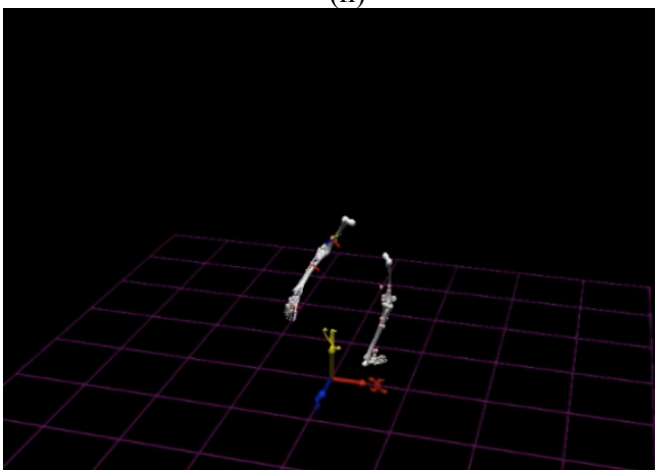

(i)

(c)

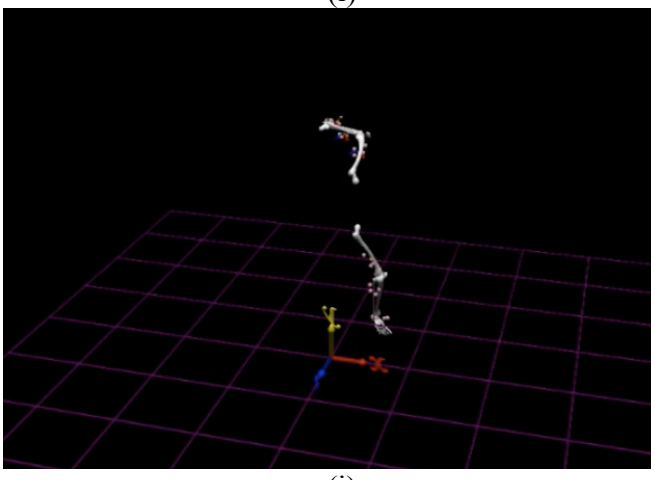

(j)

(d)

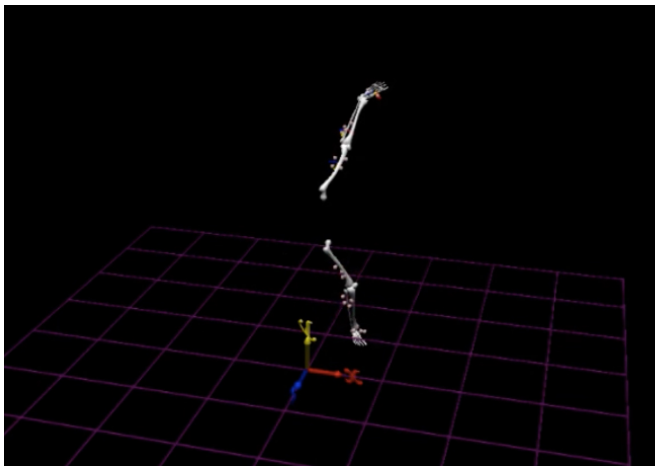

(k)

(e)

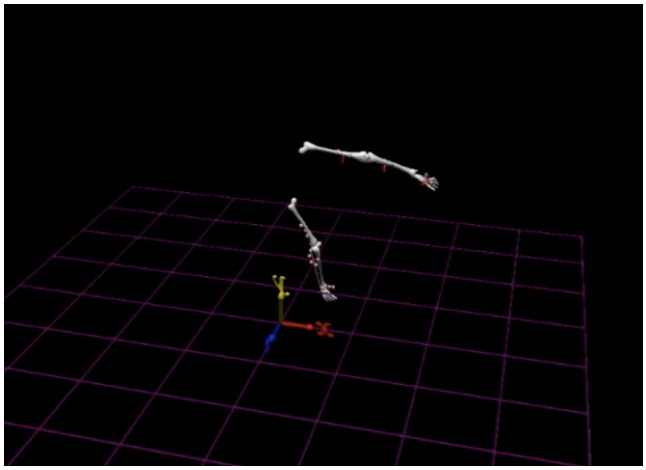

(l)

(f)

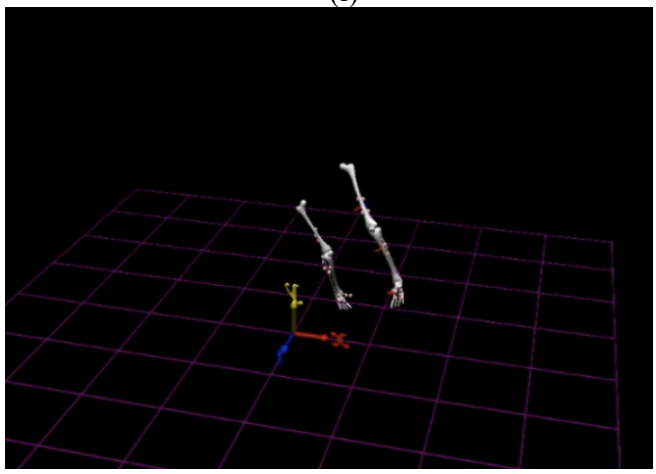

(m)

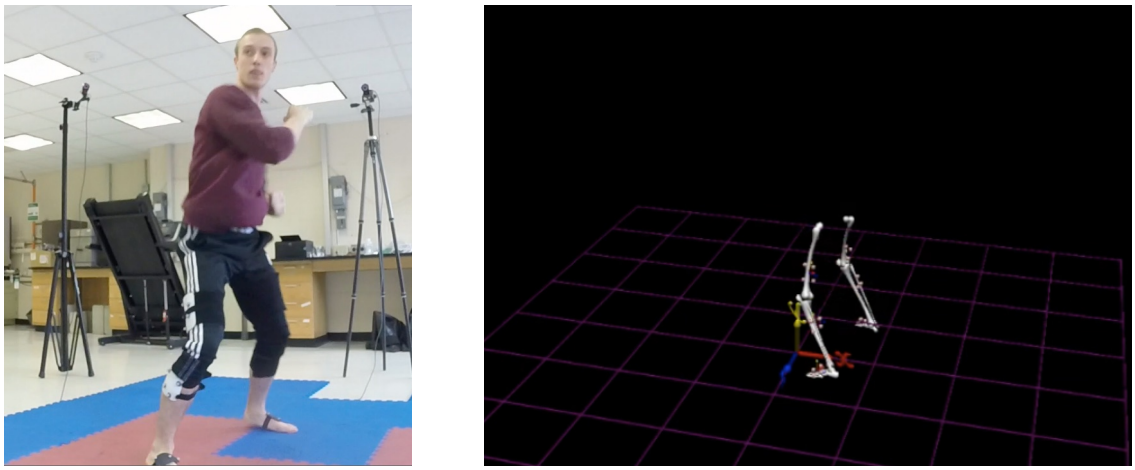

(g) (n)

Fig 18. GoPro video screenshots (a-g) and corresponding synchronized animation frames from the 3D view from Motion Monitor (h-n), for a representative *side kick* (here, with the right leg)

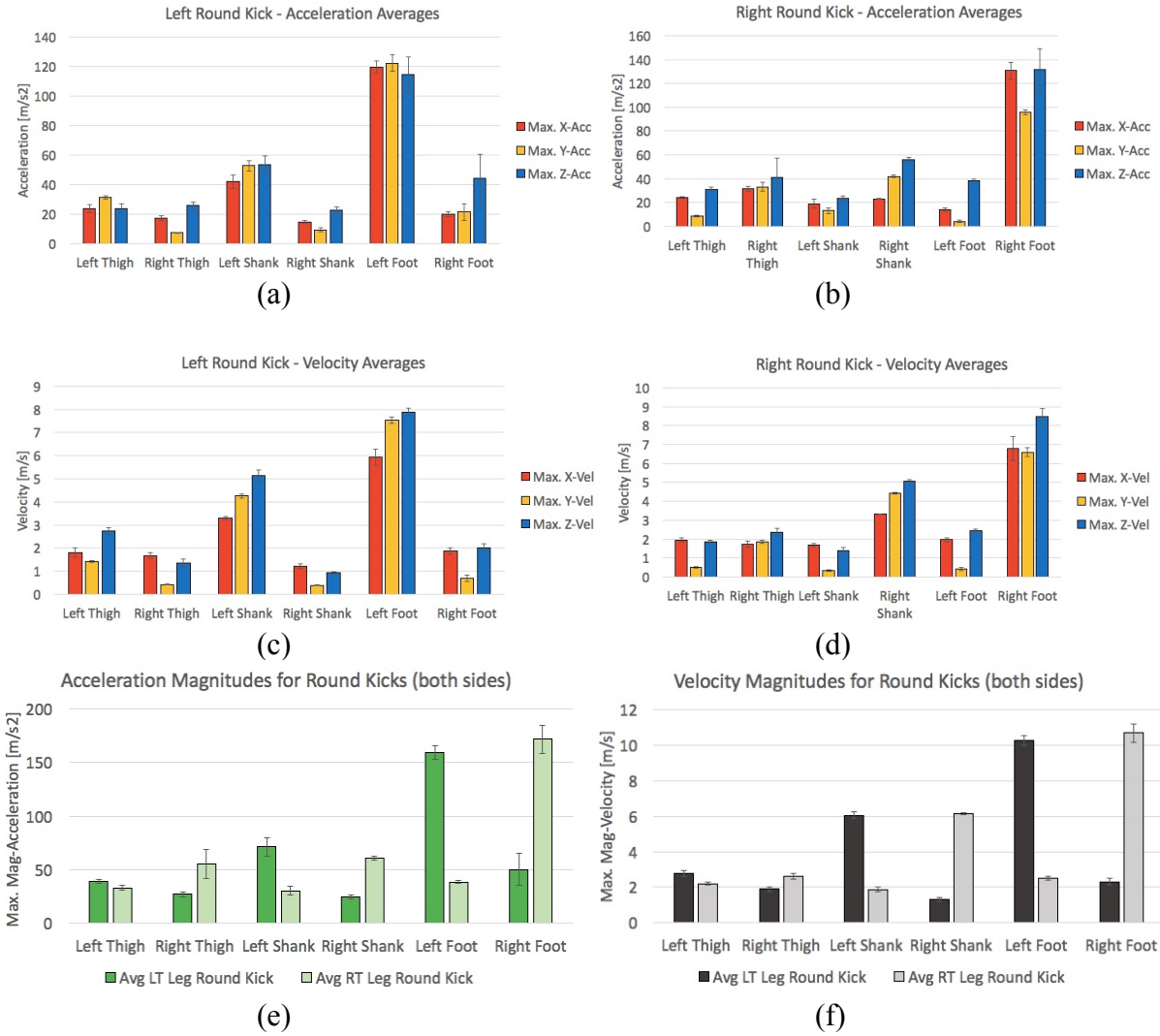

Fig 19. Summary bar graphs for maxima of x, y, z, and magnitude components of linear acceleration and velocity, averaged over all four trials of right-side and left-side *roundhouse kicks*. Error bars represent standard errors (n = 4).

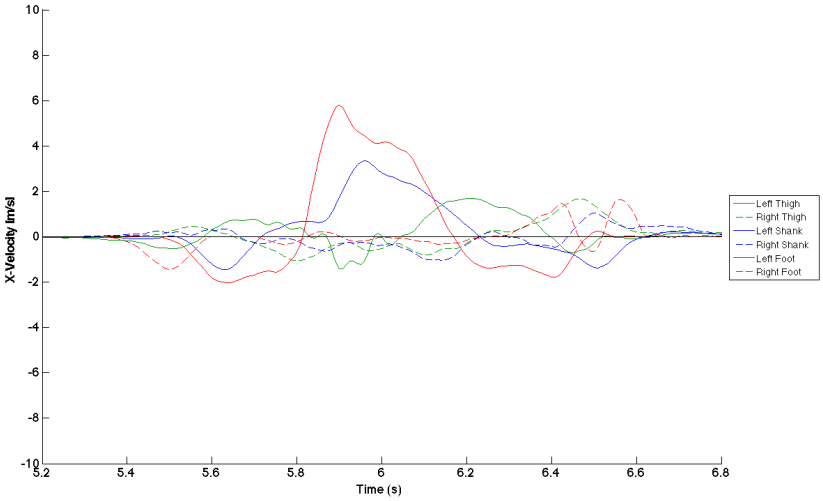

Fig 20. Example plot of the x-component of velocity vs. time for all segments, during a left-leg roundhouse kick. The movement pattern here is representative of all trials of this technique.

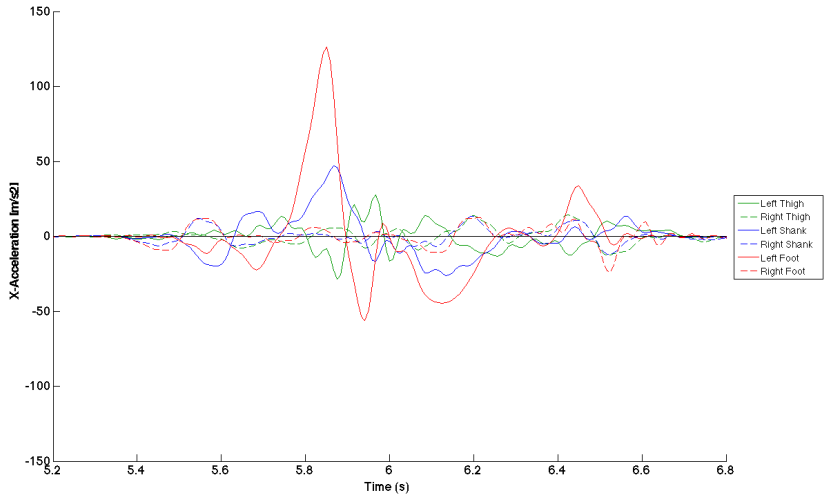

Fig 21. Example plot of the x-component of acceleration vs. time for all segments, during a left-leg roundhouse kick. The movement pattern here is representative of all trials of this technique.

Spinning Hook Kick

(a)

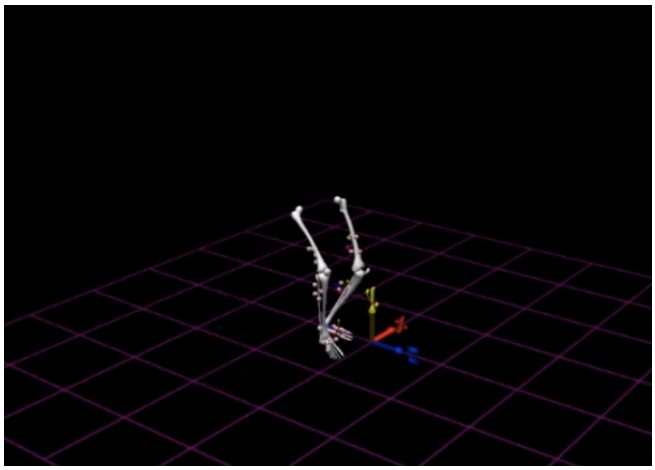

(g)

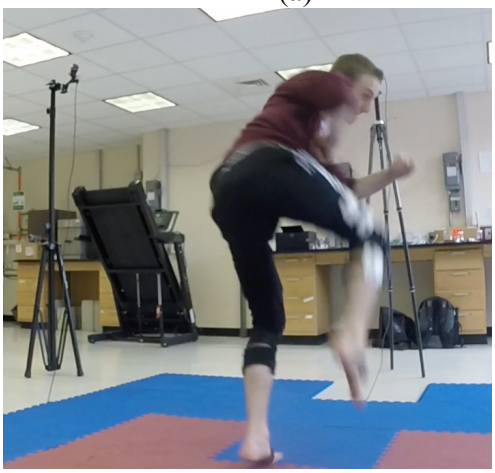

(b)

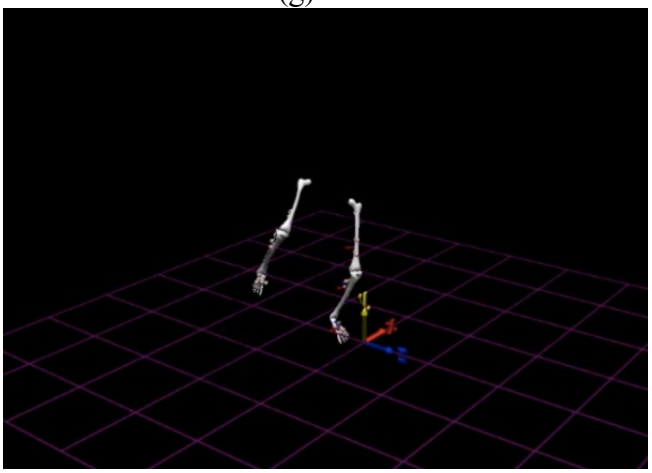

(h)

(c)

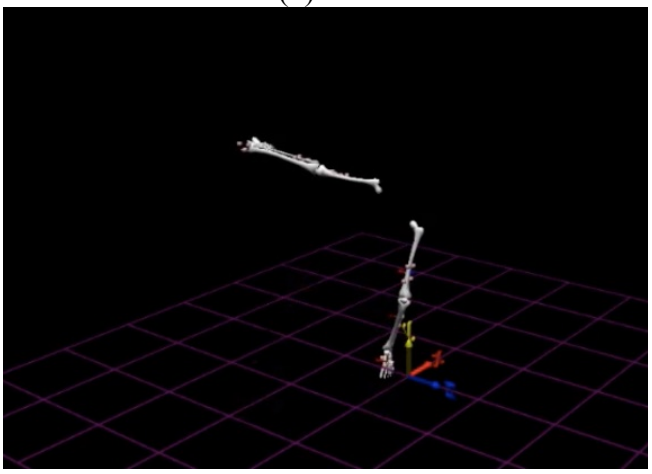

(i)

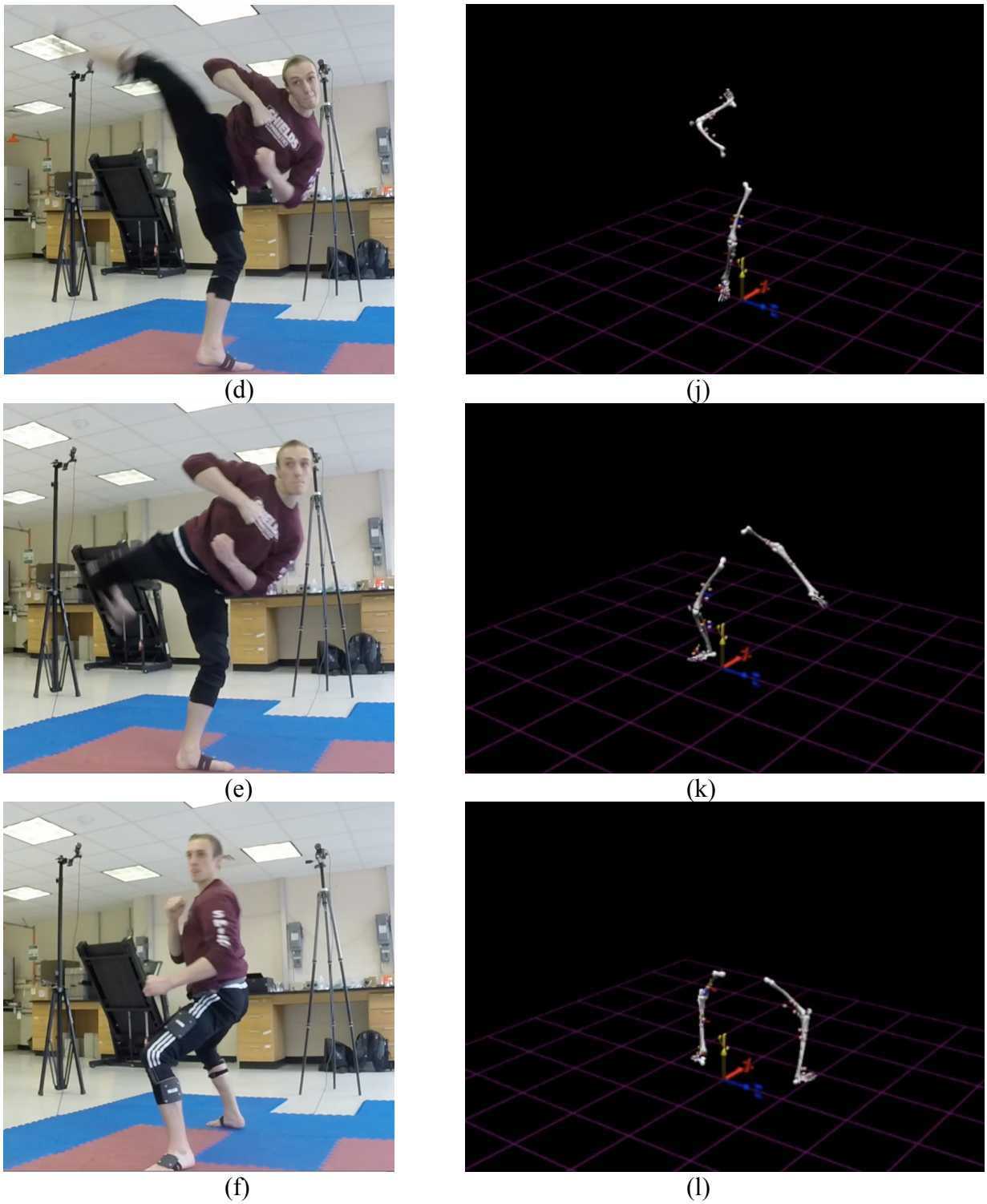

(d) (j) (e) (k) (f) (l)

Fig 22. GoPro video screenshots (a-f) and corresponding synchronized animation frames from the 3D view from Motion Monitor (g-l), for a representative *spinning hook kick* (here, with the right leg)

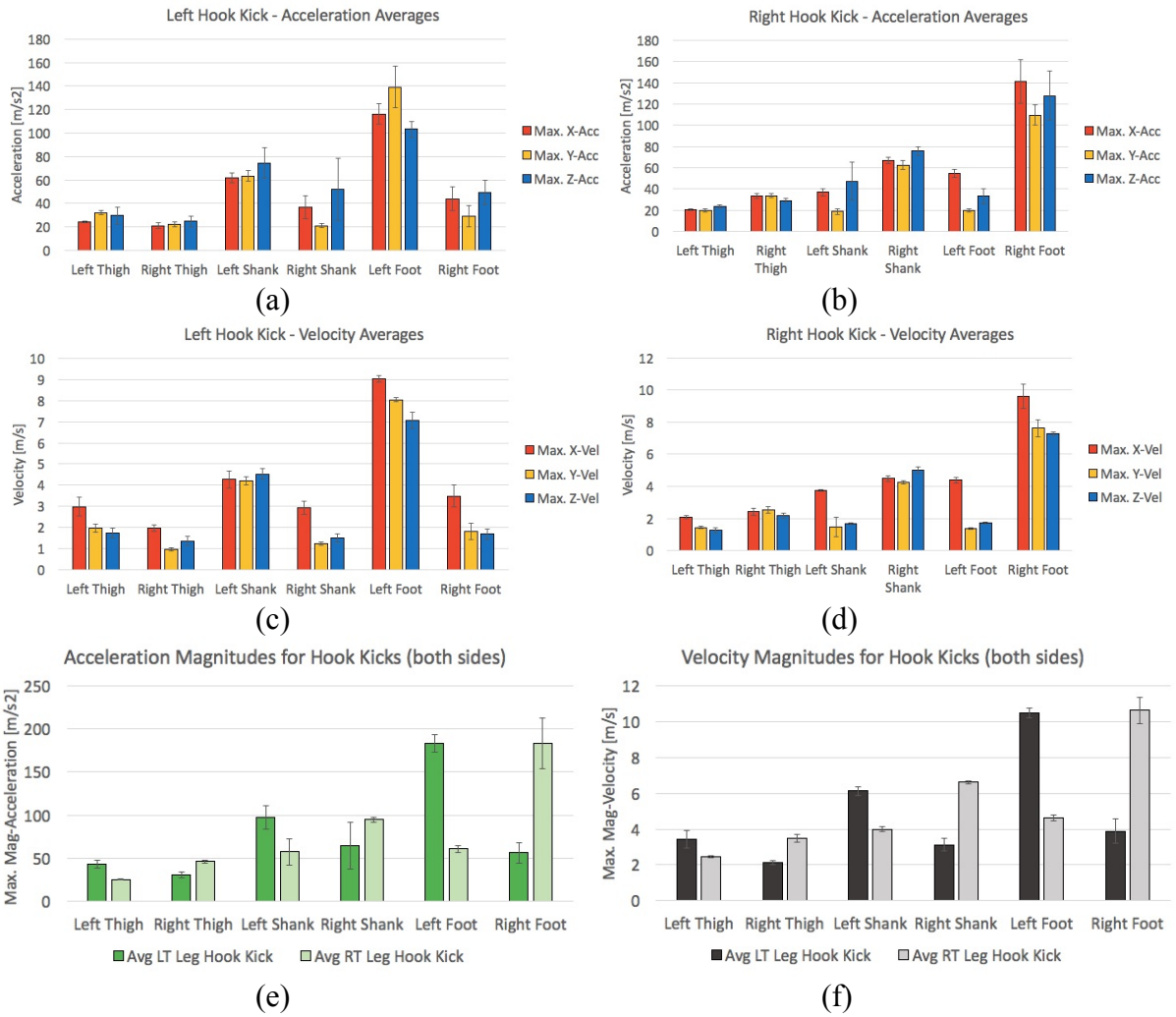

Fig 23. Summary bar graphs for maxima of x, y, z, and magnitude components of linear acceleration and velocity, averaged over all four trials of right-side and left-side *spinning hook kicks*. Error bars represent standard errors (n = 4).

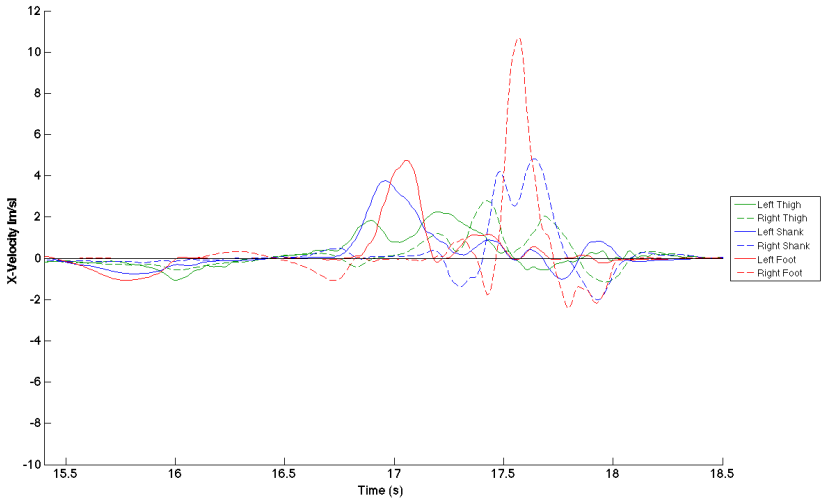

Fig 24. Example plot of the x-component of velocity vs. time for all segments, during a right-leg spinning hook kick. The movement pattern here is representative of all trials of this technique.

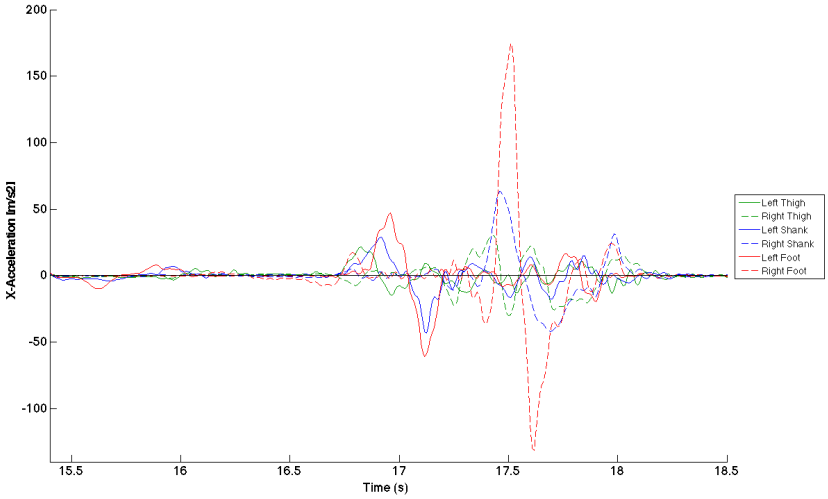

Fig 25. Example plot of the x-component of acceleration vs. time for all segments, during a right-leg spinning hook kick. The movement pattern here is representative of all trials of this technique.

Tornado Kick

(a)

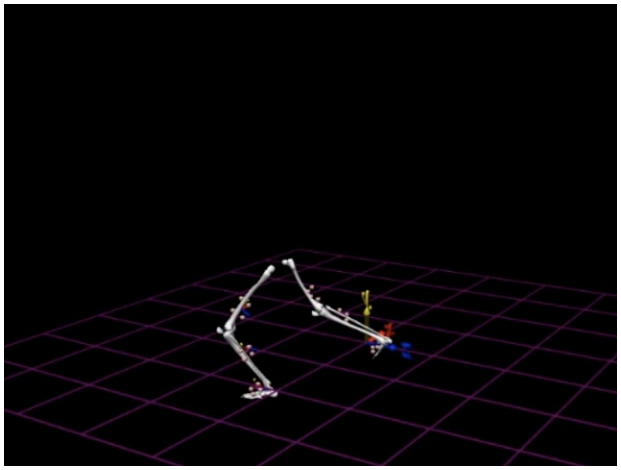

(i)

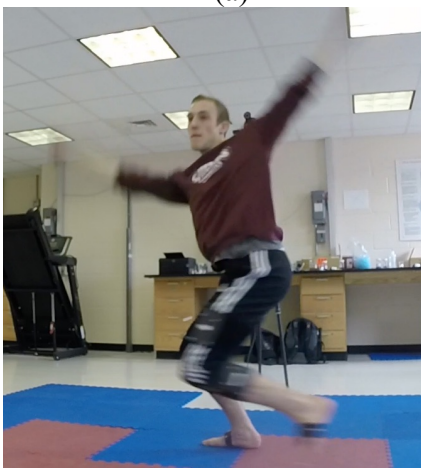

(b)

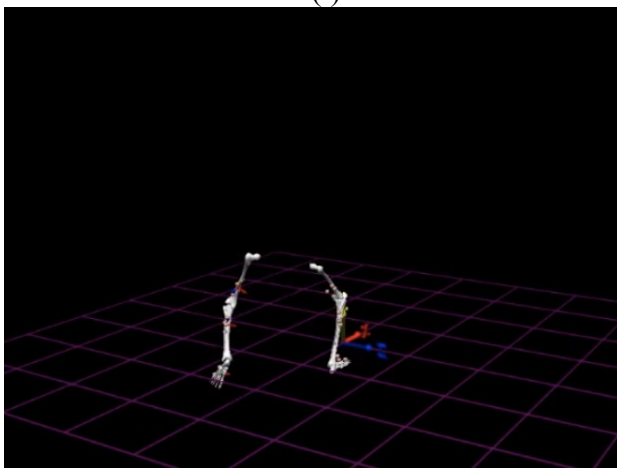

(j)

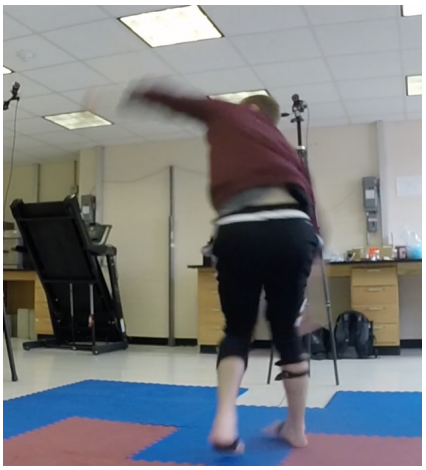

(c)

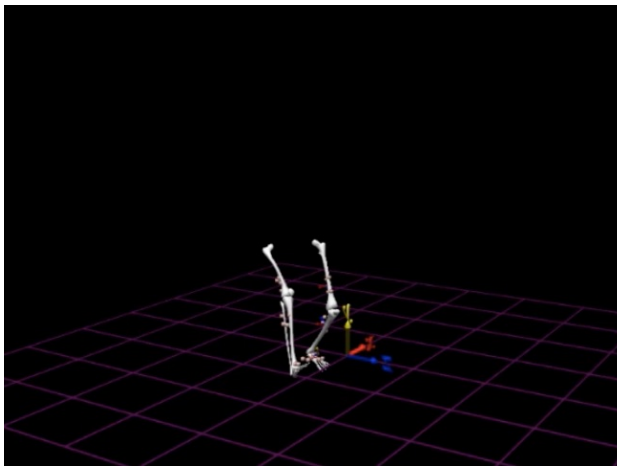

(k)

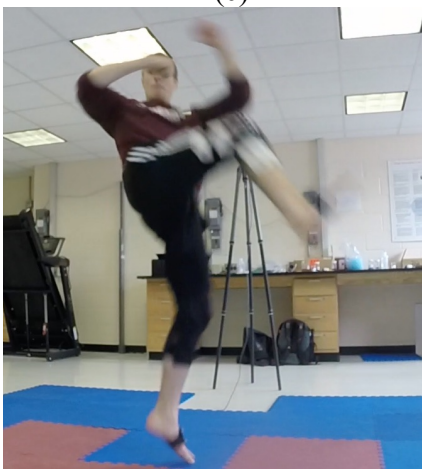

(d)

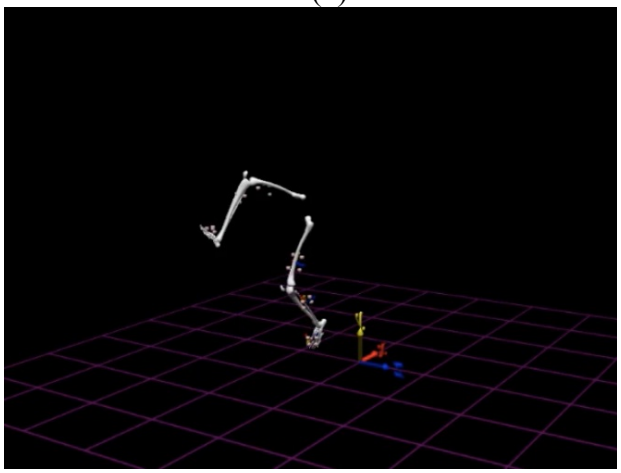

(l)

(e)

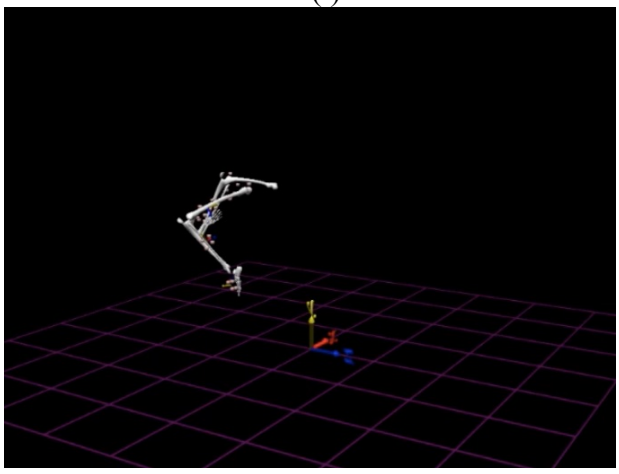

(m)

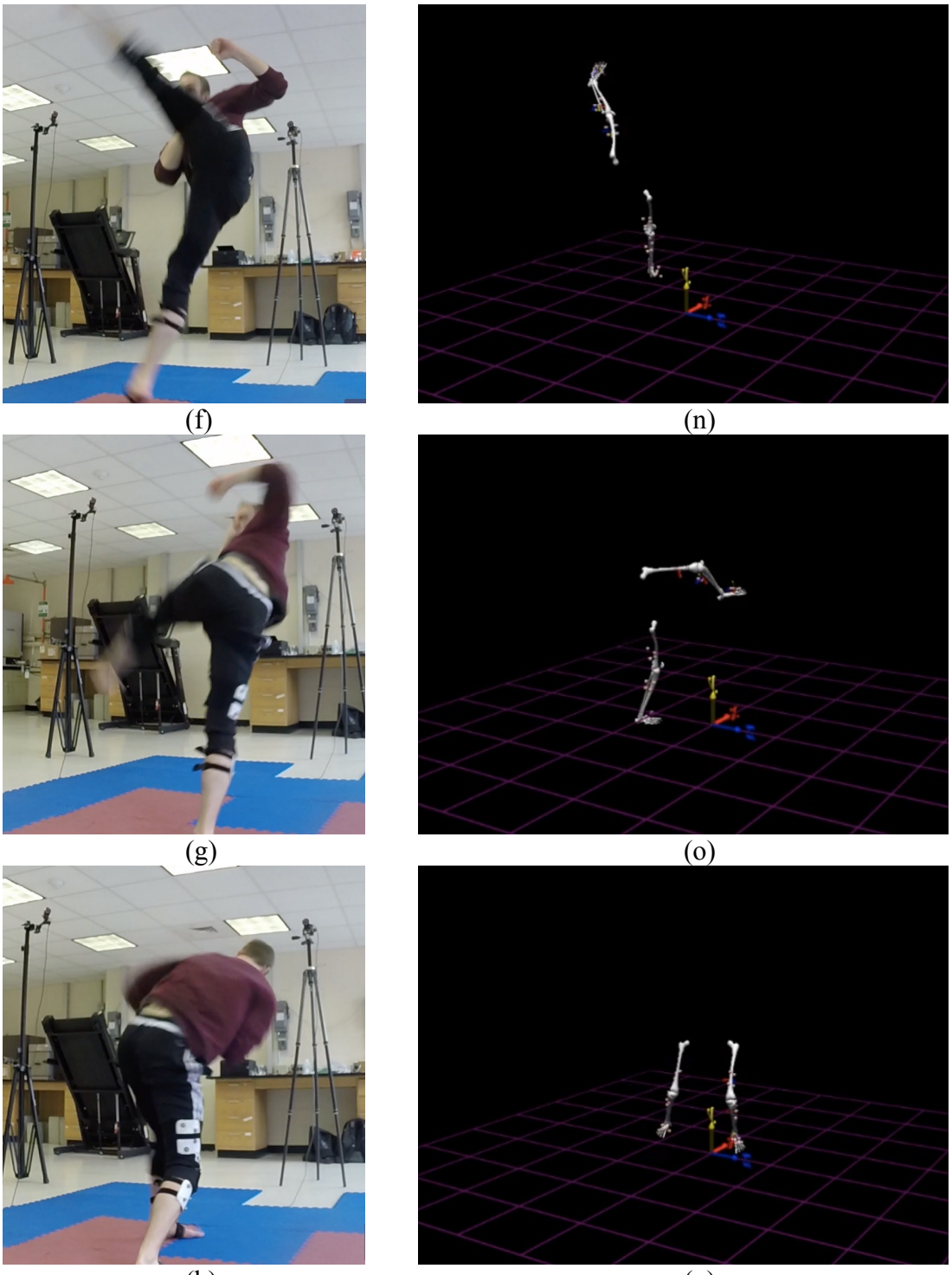

Fig 26. GoPro video screenshots (a-h) and corresponding synchronized animation frames from the 3D view from Motion Monitor (i-p), for a representative *tornado kick* (here, with the left leg)

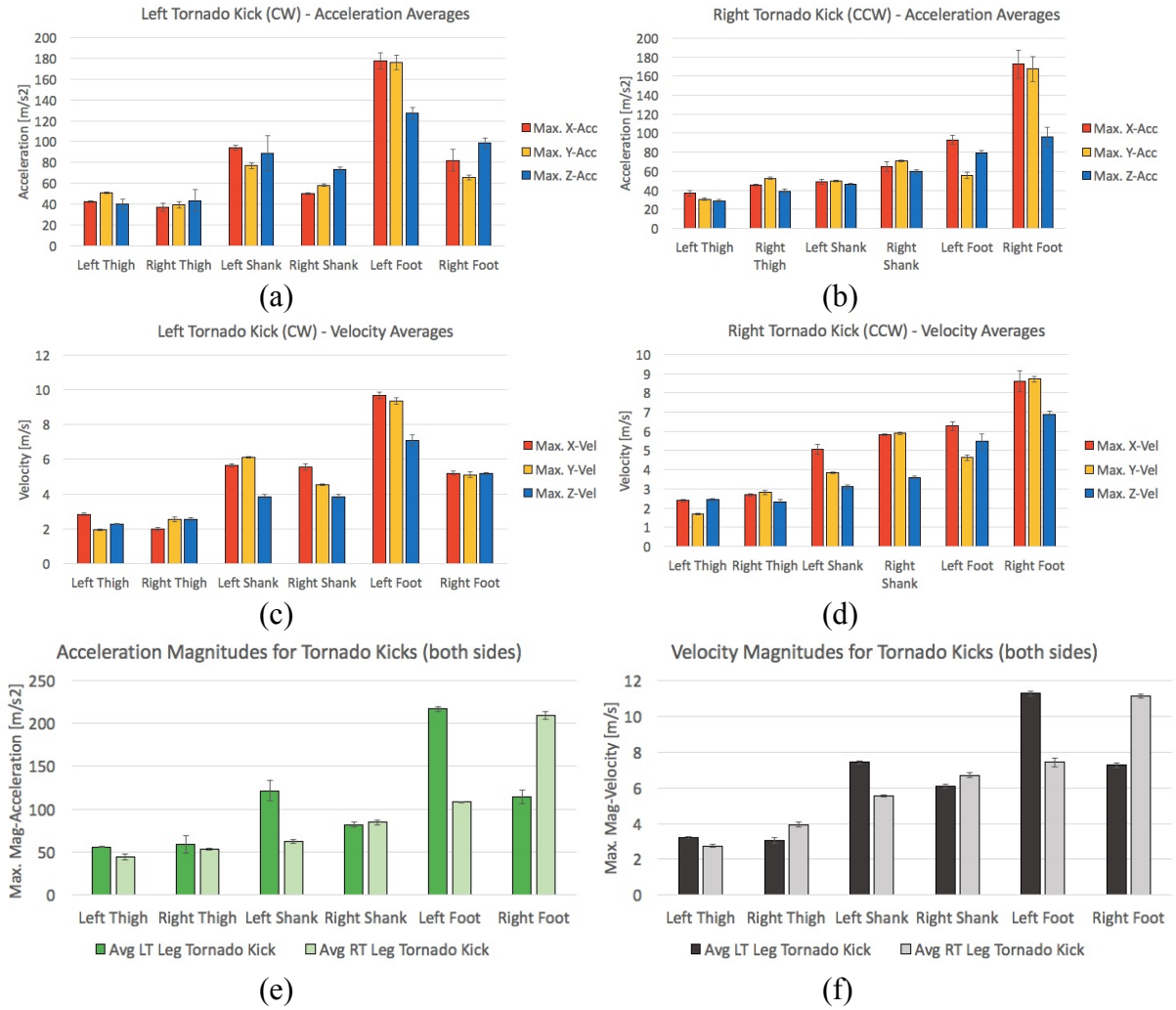

Fig 27. Summary bar graphs for maxima of x, y, z, and magnitude components of linear acceleration and velocity, averaged over all four trials of right-side and left-side *tornado kicks*. Error bars represent standard errors (n = 4).

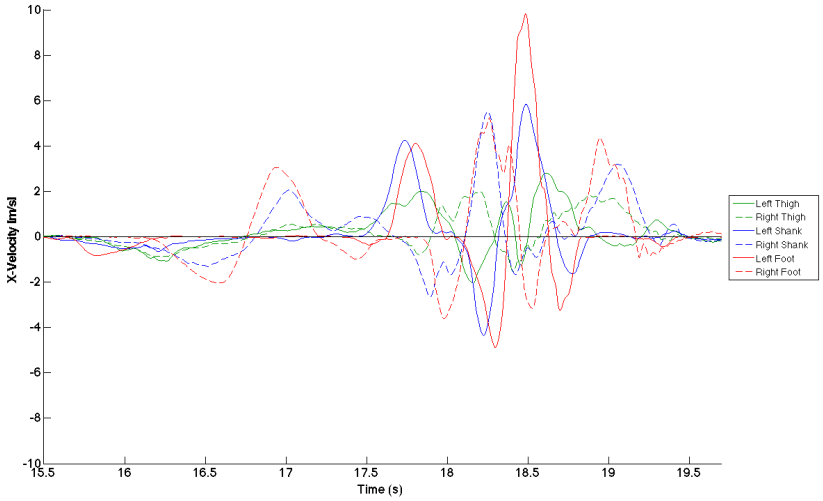

Fig 28. Example plot of the x-component of velocity vs. time for all segments, during a left-leg tornado kick. The movement pattern here is representative of all trials of this technique.

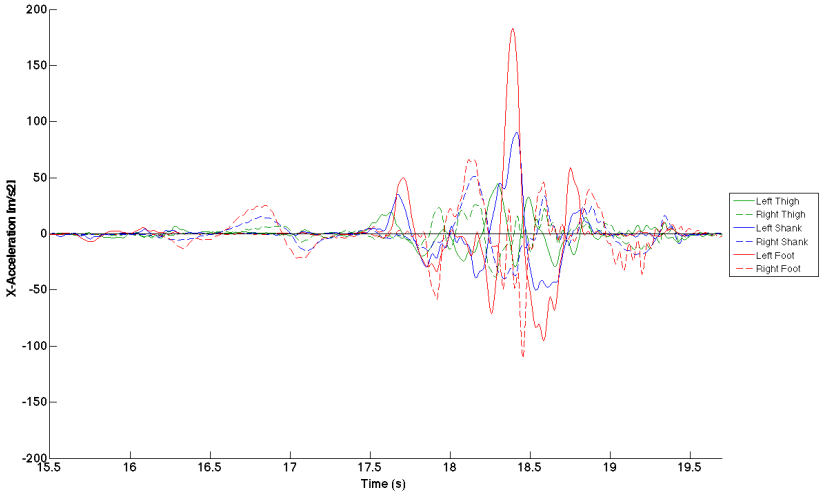

Fig 29. Example plot of the x-component of acceleration vs. time for all segments, during a left-leg tornado kick. The movement pattern here is representative of all trials of this technique.

Corkscrew (Intermediate Inverted Trick)

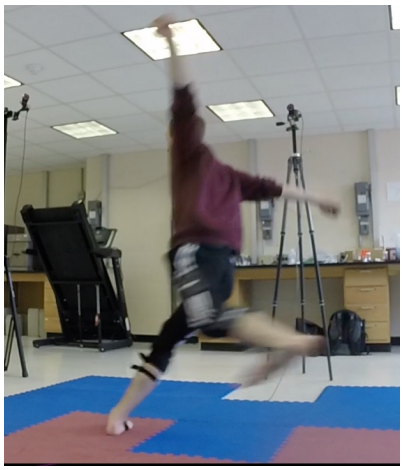

(a)

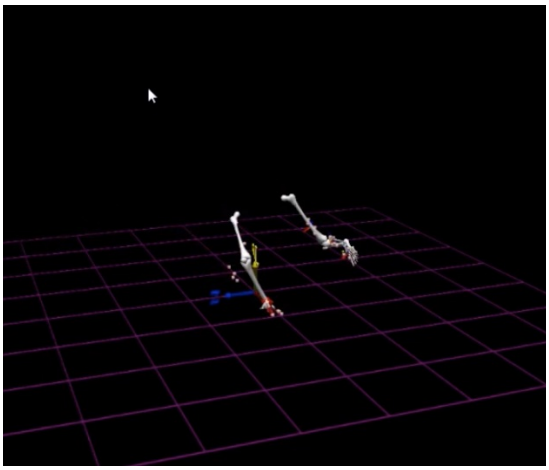

(i)

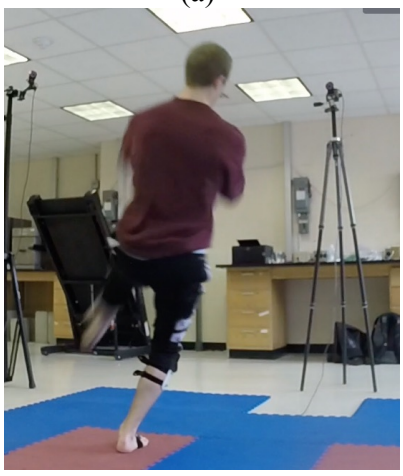

(b)

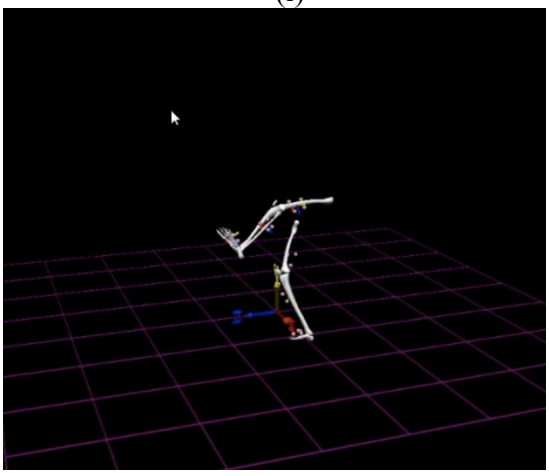

(j)

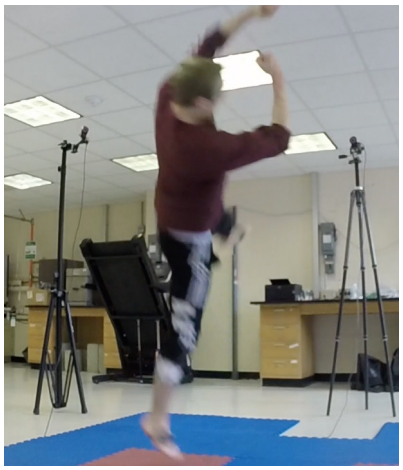

(c)

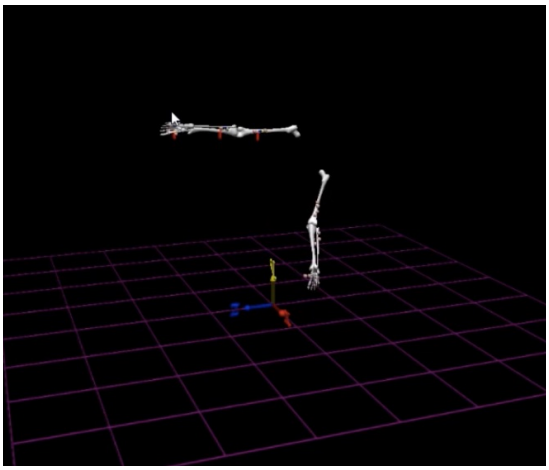

(k)

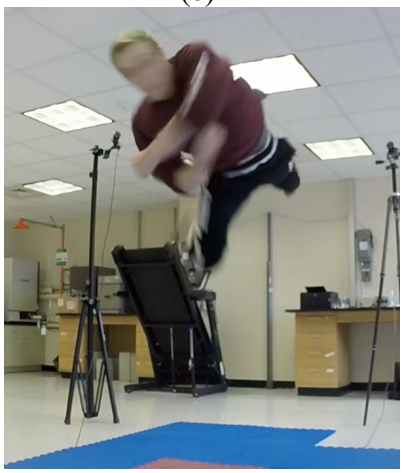

(d)

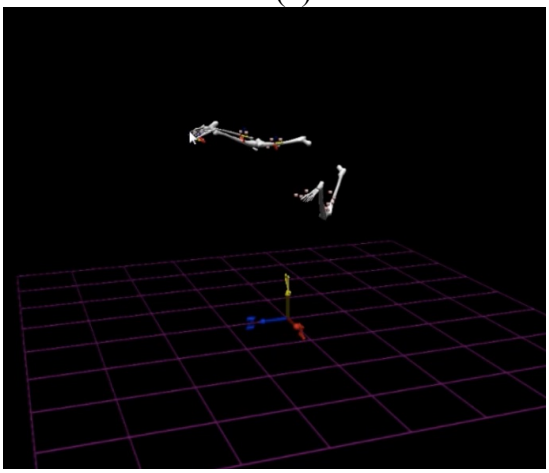

(l)

(e)

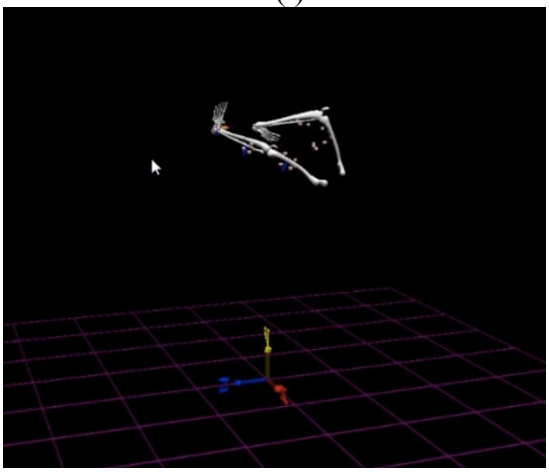

(m)

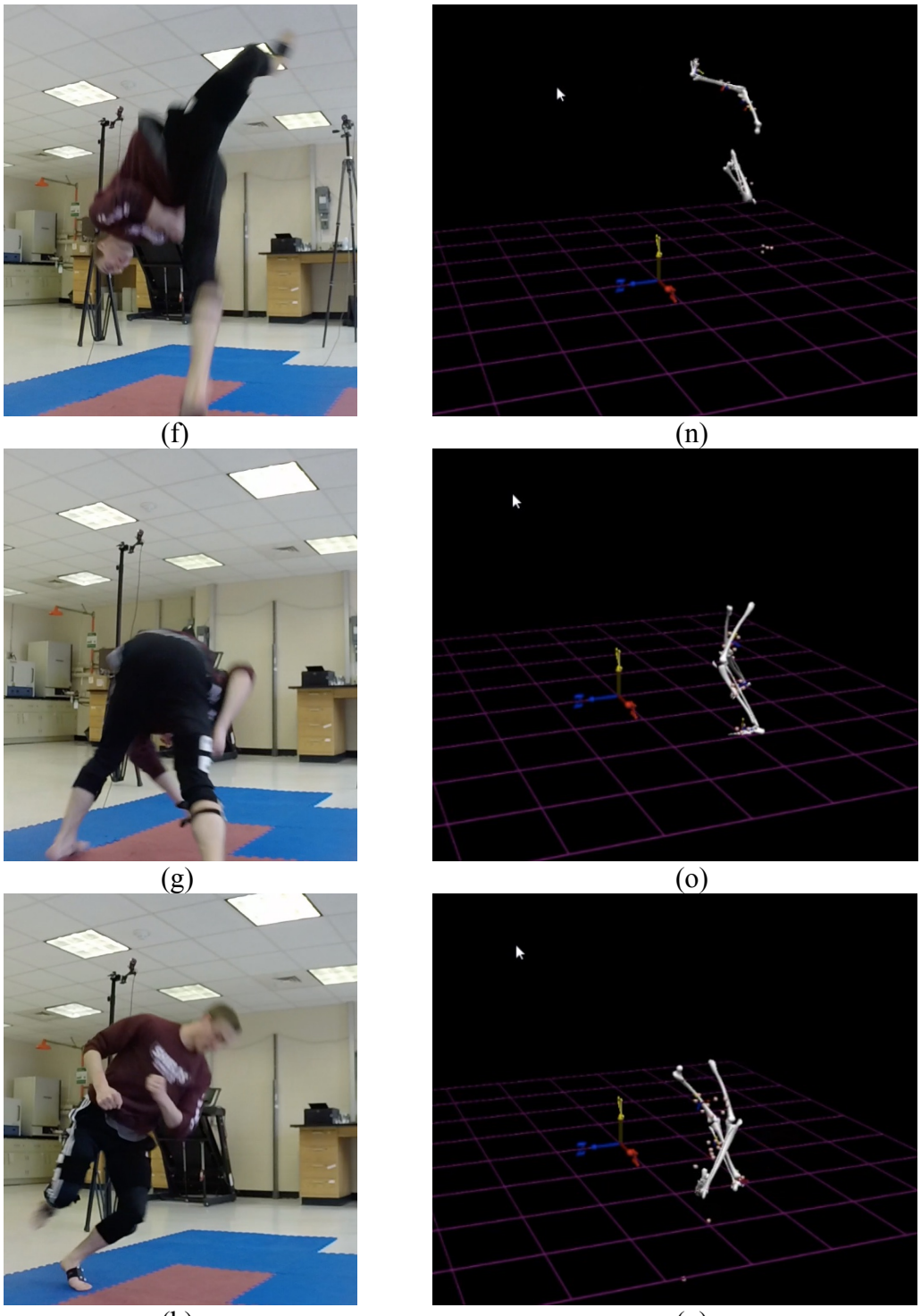

(f) (n)

(g) (o)

(h) (p)

Fig 30. GoPro video screenshots (a-h) and corresponding synchronized animation frames from the 3D view from Motion Monitor (i-p), for a *corkscrew*

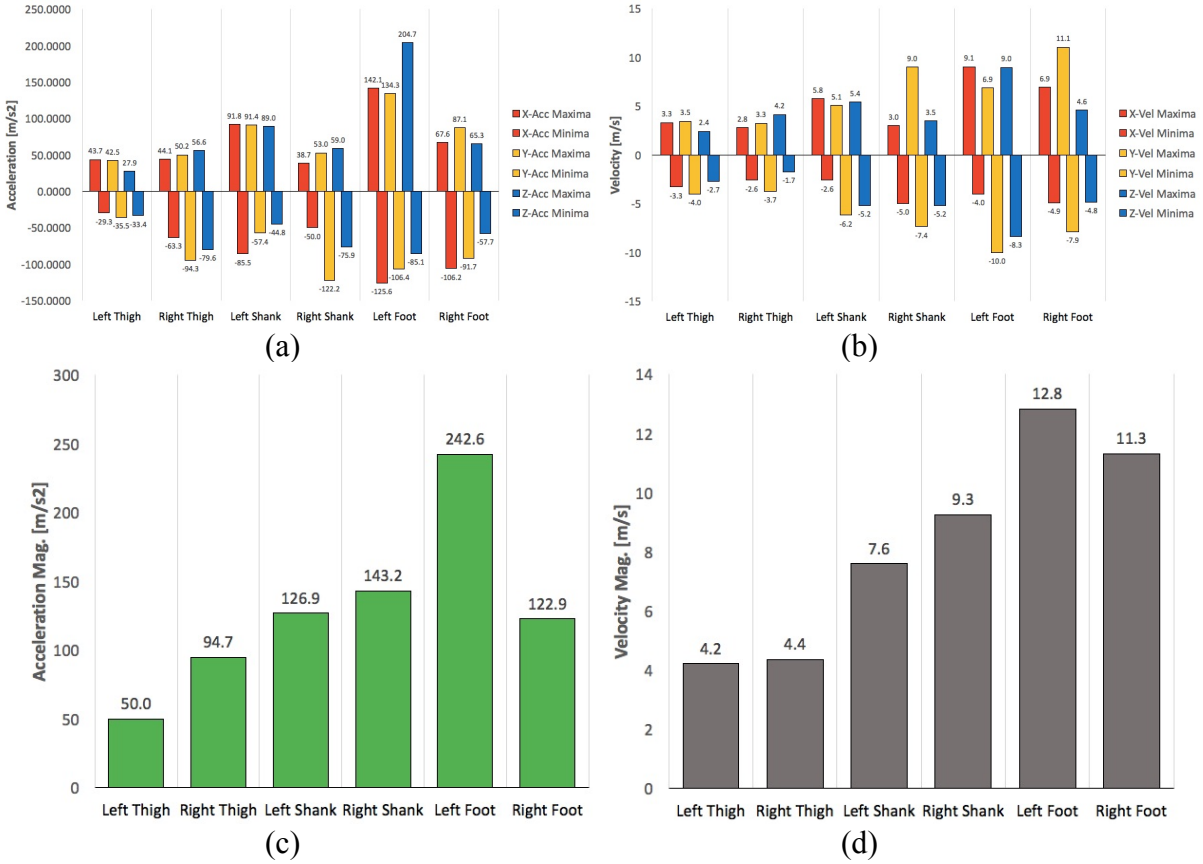

Fig 31. Summary bar graphs for maximum and minimum x, y, and z components of linear acceleration and velocity (a-b), and maximum magnitudes of linear acceleration and velocity (c-d), for a *corkscrew* performed by the subject.

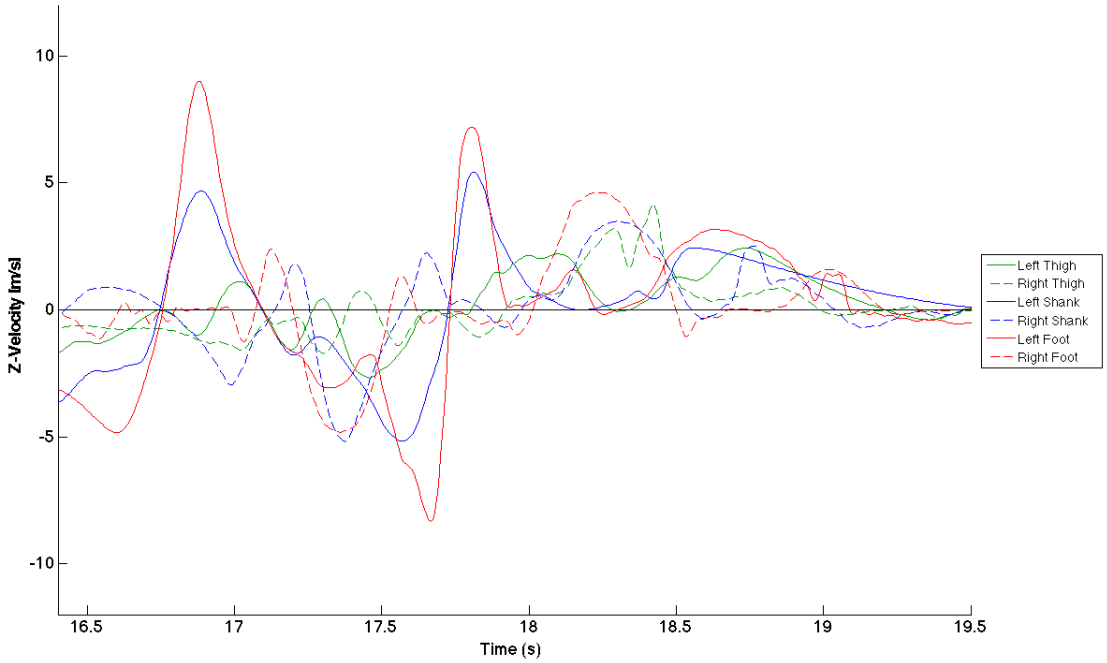

Fig 32. Plot of the z-component of velocity vs. time for all segments, during a corkscrew (CW twisting).

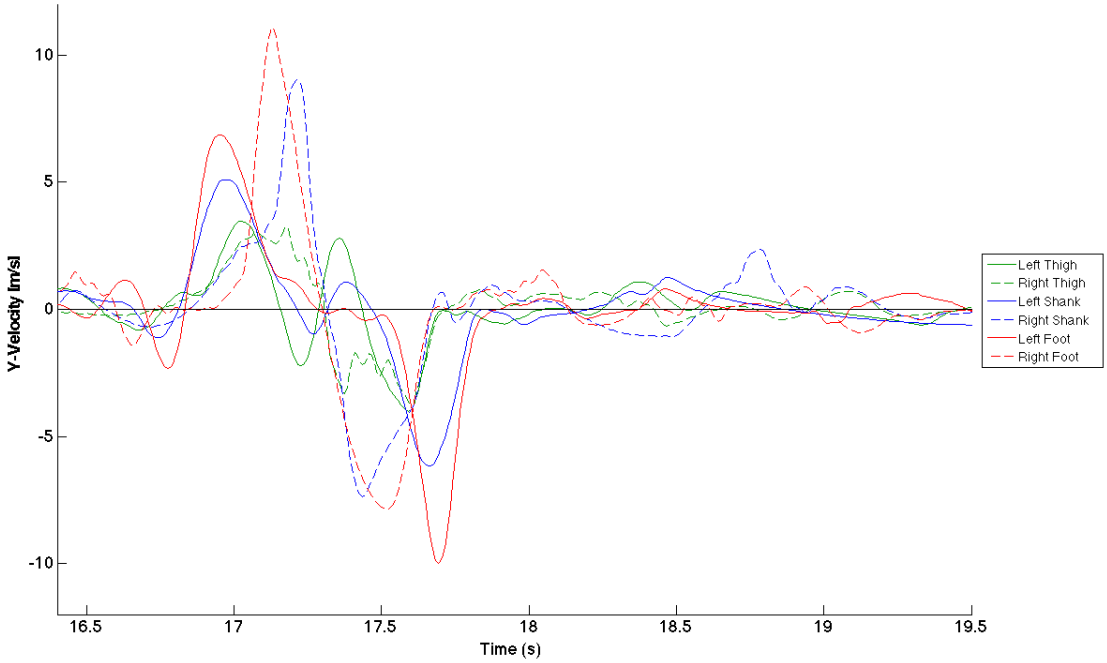

Fig 33. Plot of the y-component of velocity vs. time for all segments, during a corkscrew (CW twisting)

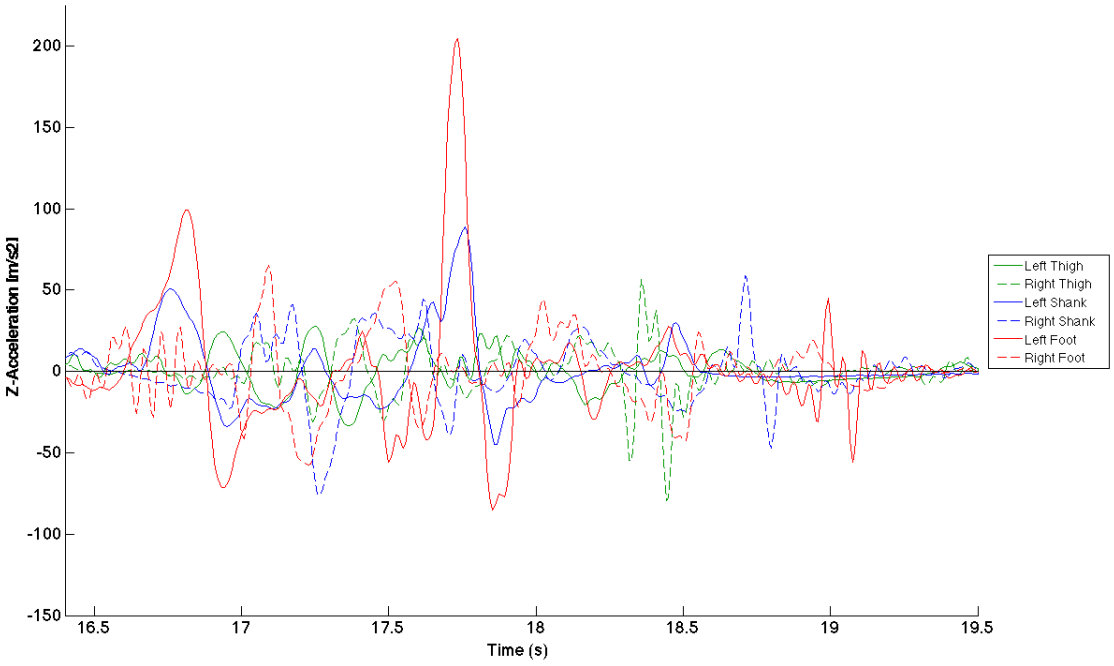

Fig 34. Plot of the z-component of acceleration vs. time for all segments, during a corkscrew (CW twisting)

IV: Discussion

The six techniques studied were four fundamental kicks in Tricking: front snap, side, roundhouse, and spinning hook, as well as one dynamic kick – the tornado kick – and one dynamic inversion trick – the corkscrew. For each technique type, synchronized key frames from the GoPro footage and Motion Monitor animation are shown side-by-side, for a representative trial for the Tricking technique. Below these images are four bar graphs that summarize the maximum, average linear acceleration and velocity components, for each body segment, for each side of doing a trick. As mentioned previously, all tricks that were performed on both sides (excluding the corkscrew) had four trials per side to average over. The last two bar graphs present the maximum magnitudes of linear acceleration and velocity for each body segment, over the duration of performance of a technique. The graphs of certain quantities that follow show the characteristic, time-dependent behavior of the kicks, in their primary directions of motion, with respect to the global axes calibrated in this procedure. The following sections break down the analysis of each of the six techniques separately and in more detail.

Front Snap Kick

As seen in the frames of Fig. 10, a front snap kick is where the kicking leg chambers with an $\sim 90^{\circ}$ angle at the hip and knee before extending the leg so that the ball of the foot strikes the target, usually in the face or body. The kick is re-chambered rapidly and placed back into stance. Fig. 10 shows that the support leg pivots slightly to allow the hip of the kicking leg to extend more violently, and provide more power to the strike. Relative to the capture environment axes, the front snap kick has minimal x-components of velocity and acceleration, where most of the motion is constrained to the kicking leg, in the y and z directions. Fig. 12 displays the z-

(anteroposterior) component of velocities for all body segments during a left-leg front snap kick. Based on Fig. 10, where –Z is the anterior direction,

Fig. 12 shows sequentially activated velocity profiles for the left and right leg thigh, shank, and foot segments. The left foot achieves the highest magnitude of z-velocity of ~8.3 m/s at the point of impact. Upon rechambering the kick, the foot rapidly decelerates and travels posteriorly (+Z) at half of the striking velocity. Again, a sequential recoil of left foot, shank, and thigh occurs, in the opposite order as the beginning of the strike. In conjunction with Fig. 12, Fig. 13 shows the anteroposterior acceleration experienced by each lower extremity segment. At the time of the strike, when the left leg is most extended, the foot is decelerating in the posterior direction at 100 m/s^2. During the buildup and recovery from the kick, the left shank is seen to achieve an acceleration of 30 m/s^2. This indicates that the acceleration of the shank causes a much higher acceleration at the striking surface itself. Therefore, the idea of chambering and snapping one's kick, while causing lower and briefer accelerations for the heavier body segments like the thigh and shank, will cause the striking foot to have destructive force and momentum transferred through it. Moreover, the acceleration spike in the left foot is due to the jerk that occurs due to the "snap" of the kick. This indicates that the knee is undergoing a large angular acceleration, because of which many athletes complain of overuse or hyperextension injuries in the knee. The kinematics here reinforce that proper training of the muscles around the knee is vital for safely performing sharp, powerful front snap kicks.

The graphs in Fig. 11 (a-d) confirm that the majority of the motion during front snap kicks is in the superoinferior and anteroposterior directions. Fig. 11 (e-f) plots indicate that for this subject, front kick performance on either side is relatively consistent and balanced. The average maximum magnitudes of acceleration for the striking foot in each case are ~150 m/s^2,

while the average maximum magnitudes of velocity for the striking foot are ~9.0 m/s. Looking at the average maximum magnitudes of acceleration and velocity for the striking leg shank between sides, it can be seen that right-side front kicks have a higher performance, with larger peak quantities in more segments of the leg than just the striking foot. For each side, the kinematic quantities of the support leg are very small, as the front kick requires a stable base from which to generate power.

Side Kick

The GoPro and Motion Monitor synchronized frames of Fig. 16 show a representative right-side side-blade kick. Here, the technique is adapted to include a pivoting stance for increased power generation; standard side-blade kicks are done while stationary, with the hip of the kicking leg already aiming towards the target. In this version, the subject takes stance facing the –Z direction. The subject's weight is shifted to the support leg as the striking leg forms a tight chambered position with a 45˚ inclination. As the striking leg prepares, the support foot pivots sharply to turn away from the target and open up the hips. Simultaneous to the pivot, the outside edge of the striking foot accelerates in the –Z direction into a thrusting strike. Recovery involves rechambering the kick and stepping through towards the +Z direction.

Just as with the front snap kick, a pattern of sequential velocity activation can be seen for the right leg segments in the z-velocity plot shown in Fig. 16. The right thigh, shank, and foot chronologically reach peak velocity, with each segment achieving a higher velocity than the last. In the side kick example of Figs. 16-17, the striking foot reaches a peak z-velocity magnitude of 9.0 m/s and a peak z-acceleration magnitude of 110 m/s^2. Again, this acceleration spike for the right foot can be traced back to a large acceleration at the knee. Due to the thrusting action of the

kick, as opposed to the snapping motion of the front kick, this acceleration at the knee is more likely to be oriented axially. The need for proper training is reinforced here, as the ligaments of the knee can be injured over time under such accelerations, without the support of surrounding muscle activity and joint stabilization. Fig. 17 also shows accelerations in the +Z direction of approximately 30 m/s^2 for the right thigh and shank, just milliseconds before the strike itself. These are indications of force transfer down the leg during the kick, as well as axial loading of the hip joint. Though these magnitudes are less severe, proper local musculature from the hip flexors and extensors is crucial for a powerful kick and joint stability.

Fig. 15 (a-d) displays bar plots that quantitatively confirm that the majority of the motion for this type of side-blade kick is in the superoinferior and anteroposterior directions. Unlike the front snap kick, the average maximum magnitudes of acceleration for the striking leg are largest in the z-direction, since the side-blade kick focuses on driving the edge of the foot forward. Any average y-acceleration maxima seen are due to the chambering process of raising the leg off of the ground. Once again, minimal average x-directional (mediolateral) accelerations and velocities are present, as the kick is stationary and requires stability from the support leg during its performance. Fig. 15 (e-f) show that the maximum magnitudes of velocity for the striking foot for the average side-blade kick on both sides is ~10.0 m/s. For the average left-side side-blade kick, the peak magnitude of acceleration for the striking foot is 160 m/s^2, while that of the average right-side kick is 120 m/s^2. These are statistically significant given the four trials tested, and could indicate underlying preferences or side-dominance for the test subject.

Roundhouse (Round) kick

The roundhouse kick is one of the two hallmark kicks from which many Tricking techniques are built upon. Many other tricks incorporate the major components of this kick and its variations during complex spinning, flipping and twisting moves too. The name "roundhouse" comes from the circumferential trajectory of the kick, where a lot of momentum is generated leading up to the kick. Unlike the previous two kicks, this technique is the first to significantly incorporate angular momentum into the strike. The conservation and manipulation of angular momentum is vital for powerful performance and successfully fluid combinations of techniques in Tricking.

Of the many styles of this kick, the one performed and presented here incorporates plantar flexion of the kicking foot, targeting at head-height, and minimal re-chambering to allow for momentum from the kick to be carried through. The frames of Fig. 18 show a representative left-side round kick performed by the subject. The starting position has the kicking leg in back, with the subject facing the –Z direction. The first event is the external rotation of the support leg where the toes of the support foot are turned outwards to open the hips and make way for the kicking leg to travel through the target. As weight is shifted onto this externally rotated support leg, the striking leg chambers at the knee with a 45˚ inclination, while the striking leg hip joint remains extended. Extension of this hip and engagement of the core muscles additionally connects the inertia of the torso into the power of the kick. In Fig. 18 (b-d), a counter-torque produced by the shoulders and arms helps the kicking leg accelerate medially (+X direction) much more rapidly, since the obliques and associated core muscles activate more forcefully as a result. The striking leg extends through the knee and ankle and maintains extension for an angular displacement of approximately 90˚, with the dorsal surface of the foot cutting through

the target at peak angular momentum. During the kick, the support foot pivots slightly with the kick so that the kick's angular momentum is sustained more efficiently. Without conventional chambering, the kicking leg is adducted towards the support leg, and the reduction in inertia about the +Y axis spins the subject rapidly back to his original stance.

In Fig. 20, the x-components of velocity for the lower extremity segments are plotted against time for a sample trial of a left-side round kick. It can be seen that the left foot reaches and sustains a peak x-velocity of ~5.5 m/s for 0.3 s. The peak velocities for the left foot and shank happen roughly at the same time, followed by that for the left thigh. Meanwhile, in Fig. 21, there is a significant acceleration and deceleration of the left foot and shank; the left foot achieves a maximum x-acceleration magnitude of 120 m/s^2. These two results together indicate that the generation of angular momentum into the kick comes from the support leg pivot and the rapid acceleration of the striking shank and foot. The late velocity peak experienced by the left thigh is due to the momentum transferred proximally, from the distal part of the striking leg, during the follow-through and recovery from the kick.

Fig. 19 (a-d) indicate significant three-dimensional motion of the kicking leg during round kicks. This can be confirmed in Fig. 18, seeing as the kicking leg follows an arc through the capture volume. Motion in the superoinferior direction is due to the hip flexion/abduction and extension/adduction during the kick. Motion in the anteroposterior direction is due to the extension of the leg towards the target. Motion in the mediolateral direction is due to the strike cutting horizontally through the target as a result of angular momentum about the longitudinal (+Y) axis. Overall, the differences in the bar plots between average left- and right-side round kicks manifest as reduced maximum y-acceleration magnitudes for the striking foot. This, among the statistically significant differences in the magnitudes of quantities overall, is most likely due

to subject preferences and bias. It should be noted that the subject was aware of his reduced stability when using the left leg as the support leg instead of the right. This led to compromises in the control of the round kick technique, causing him to systematically rush the right-side kicks. This could explain the reduced y-acceleration and velocity since rushed kicks do not achieve as high of an arc through the target. Thus, the data from Fig. 19 exhibit two different styles of kick between the right and left sides. Because of the increased stability and flexibility for the average left-side round kick, the maximum magnitudes of the quantities are lower, since a Tricking style round kick is more "floaty" and extended for aesthetic purposes. Meanwhile, the faster, sharper right-side round kicks produce, on average, higher peak velocities and accelerations for the striking leg body segments, representing more of a practical, fighting style of round kick. Thus, for this subject, average opposite side round kicks exhibit qualities of different styles, due to side-dominance and lingering effects of a past injury. Nevertheless, the maximum magnitude of acceleration for the striking foot for the average round kick on each side is ~160 m/s^2. The maximum magnitude of velocity for the striking foot during the average round kick on each side is 10.5 m/s. The increase in these velocities compared to those in previous kicks is statistically significant, given that the round kick is more dynamic and powerful than the static front-snap and side-blade kicks.

Spinning Hook Kick

The spinning hook kick is the other of the two hallmark kicks of Tricking. Just as many tricks in all three categories – kicks, flips, and twists – are built off of the principles and variations of round kicks, an equivalent set of tricks are built off of the hook kick. This kick is considered to be one of the most powerful grounded kicks possible in martial arts; it is used generously in Tricking combinations as a transition, momentum generator, or punctuation to a trick for this reason. The name "hook" comes from the type of motion of the kicking leg in the second half of the strike, where the knee flexes sharply to pull the foot past the target even faster than if otherwise. Like the roundhouse kick, angular momentum generation and conservation is crucial to a powerful spinning hook kick. The style of hook kick used in Tricking is quite particular, with some features not used in practical martial arts. First, the foot is plantar flexed to expose the heel to the target. Second, the body travels mediolaterally during the kick, in coordination with the standard direction of travel for Tricking combinations. This is because the hook kick is often used to generate momentum in the mediolateral direction for a following trick. Third, the kick itself is preceded by a step-over with the support leg, to jumpstart the 360˚ spin into the strike.

The frames of Fig. 22 show the process of a representative right-side spinning hook kick. The starting position is a staggered stance with the kicking leg in the back, facing the –Z direction. The subject winds up the shoulders and torso with a slight counterclockwise torque, while the body weight is shifted momentarily onto the left leg (support leg). The body weight is rapidly shifted back onto the right leg, as the support leg steps across to rotate the body by 180˚ about the +Y axis. The hip of the support leg also rotates internally so the toes point in the +Z direction, away from the target. This internal rotation stores potential energy in the hip rotator

muscles, to be released later during the kick. Simultaneously, the arms and torso turn during the step-over to feed momentum into the following 180˚ spin for the strike itself. Suddenly, the head turns over to spot the target in –Z, as the right hip (striking leg) is flexed and abducted to chamber for the kick. This is the point at which the stored energy from the internal rotation is released and provides the initial energy for the hook kick. The kicking leg is then extended rapidly as the leg accelerates towards and across the target, striking with the heel of the foot. A significant pivot occurs on the supporting foot, while the violent hip extension for the striking leg transfers angular momentum distally towards the foot. During the arc of the kick, the torso provides a counter-torque to maintain balance on the support leg and allow the kick to follow through its full range of motion. Near the end of the kick, after the heel passes through the target at peak velocity, the striking leg knee is flexed sharply and the associated hip remains extended; this forms the "hook" aesthetic. Tricking uses this to rapidly reduce inertia after the kick so as to return to stance or transfer the kick's momentum into another trick to follow. Practically, the hooking motion can deliver more damage to the target or simply provide a mechanism of recovery after striking a target.

Fig. 24 displays the x-component of velocity for each lower extremity segment during a sample right-side spinning hook kick. The early velocity peak for the left foot is due to the step-over preceding the kick. The peak velocity of the right foot during the kick itself is ~11.0 m/s, and is synchronized with the peak velocities of the right thigh and shank as well. Fig. 25 exhibits very interesting behavior, unseen by the other kicks. The x-component of acceleration for the striking foot reaches a large value of ~175 m/s^2 during the momentum generation of the kick itself. The powerful hip extensors such as the gluteal muscles, hamstrings, and back muscles are responsible for the distal transfer of impulse and acceleration towards the striking foot segment.

However, the secondary acceleration spike at 140 m/s^2 in the –X direction is a signature of the "hook" motion of the striking leg. This rapid acceleration is due to a powerful, angular acceleration of flexion at the knee itself. Because of the high prevalence of this technique in Tricking and hundreds of its techniques, there are athletes whose knees suffer overuse injuries or chronic irritations due to the repetitive and violent motion of a spinning hook kick. To enhance long-term performance and prevent these types of complications with joint health, proper conditioning is essential for the muscles involved in the kick and in stabilizing the knee.

The bar plots of Fig. 23 (a-d) show that the spinning hook kick involves significant motion of the striking leg in all three directions, with mediolateral motion dominant over superoinferior motion, and superoinferior motion dominant over anteroposterior motion. Therefore, the spinning hook kick has the majority of its motion in the frontal plane of the body, as expected from analyzing the technique seen in Fig. 22. Minor differences exist between the left- and right-side spinning hook kick plots in Fig. 23. While the profiles of the average maximum magnitudes of velocity components are roughly identical between left- and right-side hook kicks, the profiles of average maximum magnitudes of acceleration components are noticeably different. While the average left-side hook kick has a higher maximum magnitude of acceleration for the striking foot of 140 m/s^2 in the Y direction, the average right-side kick has higher accelerations for the striking foot in the X and Z directions, of 140 and 130 m/s^2, respectively. This can again be explained by side-dominance and the subject's kicking technique on each side. For right-side hook kicks, the GoPro and Motion Monitor footage confirmed that more emphasis was placed on tracing an arc in the XZ plane with the leg, with only enough motion in the Y direction to simply abduct the leg to kick at head-height. The subject's hips were tilted more sideways during these right-side kicks, staying true to the ideal technique of a hook

kick. However, the footage of the left-side spinning hook kicks shows that the subject's hips are slightly more square to the –Z direction, rather than tilted on an angle and allowing hip extension alone to drive the kick through. The square-ness of the hips causes the kick to become more of a crescent kick in appearance, shifting the plane of motion closer to the XY plane, rather than the XZ plane of a true hook kick.

Additionally, in Fig. 23 (e-f), statistically significant increases are present for the average maximum magnitudes of acceleration and velocity for the striking foot in spinning hook kicks on both sides, compared to those of front-snap and side-blade kicks. The maximum magnitude of acceleration for the average spinning hook kick on both sides is ~180 m/s^2, whereas the maximum magnitude of velocity for the average hook kick on both sides is ~11.0 m/s. Compared to the average round kick on either side, the average hook kick on either side has statistically significant increases in maximum acceleration magnitude only, not velocity. This is most likely due to the characteristic knee flexion and hip extension mechanisms during the spinning hook kick, which cause noticeably higher accelerations in the striking leg. However, because in Tricking the round and hook kicks are intended to be performed as temporal inverses of one another, the produce similar average maximum velocity magnitudes.

Tornado Kick (Formal Name: Cheat 360° Round)

The tornado kick is one of the introductory dynamic jumping kicks in Tricking, that teaches how to incorporate aerial takeoffs with the fundamental kicks discussed. Using the tornado kick as a basis, many other tricks can be derived by adding more degrees of rotation, higher complexity and number of kicks during the rotation, variation in the kicks, and body inversion. Therefore, this technique earns its place as one of the core kicks in Tricking. The

technique originates from Taekwondo, and can be stylized in many ways. The formal name, "cheat 360 round" allows one to infer what the trick involves. "Cheat" relates to a particular type of aerial takeoff, where some of the rotational spin – the "360" is performed on the ground prior to becoming airborne. "Round" refers to how the trick ends – with a roundhouse kick.

Fig. 26 illustrates the synchronized frames of motion for an example left-side tornado kick, which uses the left leg to strike and rotates clockwise with respect to the +Y axis. The starting position and step-over behavior is adopted directly from the spinning hook kick technique discussed (Fig. 26 a-c, i-k). In the tornado kick, however, the upper body plays a more important role during the step-over, where a purposefully large inertia in the shoulders and extended arms help generate a lot of momentum and kinetic energy into the first 180˚ of the "cheated" 360˚ spin. Once the left leg (kicking leg) is poised on the ball of the foot after the step-over, the right hip is opened in a clockwise direction while flexed sharply, to lift a straight leg high. Simultaneously, the head turns over the right shoulder to face the target, the arms lift high above the head to pull the torso into the air, and the left leg pushes strongly through the toes to create the jump (Fig. 26 c-d, k-l). The right hip opening clockwise and residual angular momentum of the upper body from the wind-up accounts for the final 180˚ of rotation about the longitudinal axis, so that the subject faces the target in the –Z direction again. The key in the tornado kick is the hip-turnover while airborne that follows the jump and final 180˚ spin. With the right hip elevated at the start of the jump, the muscles of the core and upper body are engaged at the peak of the jump to elevate the left hip above the right hip. With the striking hip now elevated and aimed forward, the left leg extends violently, with aid from the body's angular momentum to perform a left-side round kick (Fig. 26 d-f, l-n). At the same time, the right leg extends down towards the floor to brace for the single-leg landing, while the kicking leg follows

through, in anticipation of using the momentum for following tricks in a combination (Fig 26 f-h, n-p).

Fig. 28 shows the x-velocity as a function of time for all lower extremity segments for a sample left-side tornado kick. The complicated series of peaks and valleys is due to the multiple phases of motion during the tornado kick. The small activity of the right leg from t = 16.3-17.3 s is due to the subject winding up and settling into stance prior to executing the technique. The second peaks, now for the left shank and foot, at t = 17.5-18.0 s, correspond to the step-over in the "cheat" setup. Next, two out-of-phase velocity patterns occur with the segments of both legs. The pattern is in the shape of a sinusoidal "letter W" in x-velocity, hinting towards the rotational motion in the XZ plane of the body during the kick. The right leg (dotted lines in Fig. 28) completes the pattern slightly before the left leg, reflecting the fact that the right leg traces its arc just before the striking leg traces through. The peak x-velocity of the left leg strike for this tornado kick trial is ~10.0 m/s. The x-accelerations in Fig. 29 show three main features. The right leg lifting during the jump in the "cheat" setup experiences a peak x-acceleration for the right foot of ~60 m/s^2 in the +X direction. The striking foot then experiences a peak x-acceleration of ~180 m/s^2 in the +X direction, whereas the right foot preparing for landing experiences an x-acceleration of ~110 m/s^2 in the –X direction. The main takeaway from Figs. 28-29 is that the oscillating accelerations and velocities, exchanged between extremities on each side, accumulate momentum and energy that culminate into the final strike, where the peak quantities are present. In Tricking, the setups and transitions between tricks are everything, when it comes to effective performance, control, and use of momentum to execute multiple tricks in a row. This is quantitatively evident in Figs. 28-29.

Fig. 27 (a-d) indicates that the tornado kicks primarily involve motion in the XY plane, whereas z-directional motion is less dominant on both sides. This is reflected in Fig. 26, where the subject does not travel much in the anteroposterior (±Z) direction, as this is generally not the goal when most Tricking combinations direct translational momentum mediolaterally. These bar plots also show that, besides minor differences in the average maximum magnitudes of acceleration and velocity components for the kicking-leg shank, the profiles for tornado kicks on each side are nearly identical. This can be attributed to the subject's ability to mirror this technique well on either side.

Fig. 27 (e-f) shows the average maximum magnitudes of acceleration and velocity for tornado kicks on both sides. The average maximum magnitudes of acceleration for the striking foot, on each side, are ~220 m/s^2. The average maximum magnitudes of velocity for the striking foot, on each side, are ~11.2 m/s. Based on the standard errors displayed on these plots, and comparing with the plots of previous kicking techniques, the tornado kick has statistically significant increases in average maximum magnitudes of acceleration and velocity. The most probable hypothesis is that jumping kicks such as the tornado kick achieve higher peak accelerations and velocities, on average, due to the dynamic nature of these advanced kicks and the energy required to get airborne. For the purposes of Tricking, the goal is to perform sequences of these airborne kicks and/or flips with kicks. Therefore, the large kinematic and dynamic quantities associated with these airborne techniques are important for understanding what loads are applied to the musculoskeletal system and how to address injuries within the sport. For the purposes of self-defense and traditional martial arts, however, airborne kicks like the tornado kick are often too costly, leaving the fighter vulnerable for counter, despite the possible enhancements in striking force and kinetic energy.

Corkscrew

The corkscrew is an example of an intermediate-skilled inversion trick, which blends rotation on all three axes. The majority of the motion occurs along the frontal and longitudinal axes. This trick is derived from Capoeira, where martial arts is combined with music and dance into acrobatic movements, similar to those found in Tricking. Corkscrews are popular among Tricking athletes because of their aesthetic appeal and momentum generating abilities for later tricks in a combination. Fig. 30 shows the frame-by-frame breakdown of a clockwise-twisting corkscrew as seen by the GoPro and Motion Monitor. The subject begins with a turning, hop-step (not seen in Fig. 30) to generate angular momentum along the +Y axis. Just before the takeoff, the right foot is planted out in front of the body's center of mass, with the right hip externally rotated 90˚. The left leg (swing leg) traces a low, diagonal arc past the right leg, while the left hip turns clockwise to square up with the right. The corkscrew takeoff involves a synchronized forward and upward swing of both arms and the left leg, while pushing through the right foot to jump into the air (Fig. 30 b-c, j-k). The swing and jump motions launch the body's center of mass into the air, while generating substantial angular momentum about the frontal axis to initiate a backflip. The swing leg trajectory is aimed across the front of the body towards the opposite shoulder, to allow the axis of flip to be tilted in the frontal plane. To engage the twist along the longitudinal axis during the flip, the shoulders and right leg wrap in tightly (Fig 30. d-f, l-n). Pulling back with the right arm, punching across the torso with the left arm, and turning the head, causes the shoulders violently rotate clockwise into the twist. The core muscles are engaged such that the shoulders and hips twist in unison. The hip twist is reinforced by reducing the right leg's inertia at the peak height of the trick (Fig. 30 e, m). After the 360˚ longitudinal twist, the subject spots the landing and the right leg accelerates towards the ground to meet the

landing. The single-leg landing of a corkscrew is common for inversion techniques in Tricking, as it allows the swing leg to follow through conserving the angular momentum of the flip. This momentum can be used to link many repetitions of the same trick, or transition into different techniques or planes of motion.

Figs. 32-33 show the z- and y-components, respectively, of velocity for all lower extremity body segments during a clockwise-twisting corkscrew. The three major z-velocity spikes seen in Fig. 32 belong to the left shank and foot, due to the powerful swing backwards (+Z) in the corkscrew setup, and the swing-through (–Z then +Z) during the recovery of the corkscrew. The peak z-velocity of the left foot during the swinging takeoff is ~9.0 m/s in the –Z direction, while during the swing-through it is ~9.0 m/s in the +Z direction. In between these two spikes, for a time interval of approximately 0.5 s, the z-velocity of the left leg becomes less than that of the right leg. This is the moment where the swinging leg remains relatively fixed in the air, while the body twists around it. For the corkscrew technique presented here, the subject consciously locks out the left leg by tensing the quadriceps, gastrocnemius, gluteal muscles, and core muscles, so that the leg is rigidly fixed with the center of mass, which is nearly motionless at the peak of the jump. Fig. 33 displays this behavior too, where the solid lines of the left leg segments have a flat-lined y-velocity in between the swinging takeoff and the swing-through landing. The peak y-velocity for the swinging foot is ~6.0 m/s in the +Y direction (superior), whereas that during the landing of the trick is ~10 m/s in the –Y direction (inferior), in order to rapidly brace for impact. However, unlike in Fig. 32, the y-velocities of the right leg become very large for a brief period while the left leg is nearly motionless in the Y-direction. This behavior corresponds to the right leg tucking in and wrapping over top of the fixed, left leg axis (see Fig. 30 c-f).

Compared to the techniques previously analyzed, the corkscrew has several instances of significant segment acceleration, shown in the z-components in Fig. 34. First, the left leg swinging into the +Z direction produces an acceleration in the left foot of ~100 m/s^2. A jerking deceleration of 80 m/s^2 into the –Z direction for the left foot indicates the moments just prior to fixing the left leg in the air as the twisting axis. Upon landing, a large acceleration of ~200 m/s^2 is produced in the +Z direction, which generates the powerful momentum used for swinging through into another trick after the corkscrew. A similar magnitude of acceleration is experienced by the right leg upon landing. This type of high-speed, dynamic, single-leg landing is particularly interesting for studying the loads involved in the ankle, knee, and hip during Tricking landings. Contrary to gymnastics and other sports, the significant forces and impact energies associated with acrobatic movements are frequently concentrated into a single leg. Moreover, many athletes must absorb such impacts and immediately produce strong jumps off of the same leg, to continue a combination. Particularly for the corkscrew performed here, the right leg must absorb all of the impact momentum and energy and regenerate more to lift the body into another corkscrew, for example. Many examples of this concept exist on YouTube; for example: https://www.youtube.com/watch?v=xU7-yy7U2rw shows one athlete, Bailey Payne, performing 25 corkscrews in succession, using the swing-through to transition between each one. As another example, https://www.youtube.com/watch?v=fzPUaHLNVsg shows Ilya Vtorin performing 25 gainers (corkscrew without the twist) in succession. Both athletes have clearly mastered muscular control and joint stability in their jumping leg.

To summarize the corkscrew analysis, Fig. 31 displays bar plots. Given that only one trial of data for the corkscrew was acquired, the values may not be representative of the subject's average performance, and certainly not of the performance of the average Tricking athlete.

Nevertheless, the data serves to give a preliminary view of the kinematics involved in the corkscrew. Fig. 31 (a-b) shows that the maximum component magnitudes of acceleration and velocity during the corkscrew are largest in the x- and z-directions for the left foot segment, and largest in the y-direction for the right foot segment. The peak velocity magnitudes for each foot segment are approximately 10-11 m/s. The differences in axis dominance between right leg and left leg segments reflect the knowledge that the swinging left leg travels fastest when its arc aligns with the x- and z-directions, whereas the jumping right leg travels fastest in a vertical arc over the left leg twisting axis. Overall, the maximum magnitudes of acceleration and velocity for the lower extremity body segments are noticeably larger than the less demanding and acrobatic techniques analyzed in previous sections. For example, the left foot and right foot achieve maximum velocity magnitudes of 12.8 and 11.3 m/s, while the maximum acceleration magnitude of the left foot reaches 242.6 m/s^2.

V: Conclusions

Overall, this report presents a methodological framework for analyzing the complex, dynamic movements of Martial Arts Tricking. Of the six techniques analyzed, various kinematic principles were discovered about how the techniques are performed, what accelerations and velocities are generated, and how momentum is transferred. The limitations of this study are due to only one subject being analyzed. Certainly, studying the same six techniques when performed by many different Tricking athletes can provide more accurate comparisons of the kinematics and dynamics of the tricks. Moreover, more trials on different days and with different conditioning regiments for a single subject can result in more accurate quantitative representations of the subject's performance capabilities and personal technique in performing

each skill. This can allow for comparisons in technique between different athletes and body-types, to get a more comprehensive view of Tricking as a whole. In the future, it would be beneficial to use more motion capture markers on more body segments, to capture the dynamics of the entire body during tricks. This is important for the overall analysis of Tricking since many skills require effort from all body segments.

The preliminary findings presented here can be extended for further investigations of Tricking biomechanics. For example, electromyography could be paired simultaneously with motion capture, to study the time-dependent muscle activities responsible for generating and absorbing momentum in different Tricking skills, transitions, and landings. Additionally, force/torque sensors on the mats beneath the athlete could measure the reaction forces applied to the body, to trace loadings at the various joints of the lower extremities.

Analyzing Martial Arts Tricking using motion capture, electromyography, and force-torque data acquisition is clinically relevant because it can improve our understanding of the biomechanics of the relatively young, high-intensity sport. From within the athletic community, it is well known that Tricking requires significant strength, flexibility, coordination, and conditioning, to remain safe and effective at the sport for many years. Tricking offers an exciting new application for biomechanical investigations, both to further understand the capabilities of the human body in sports and to potentially design conditioning regiments, rehabilitative therapy protocols, and orthopedic treatments that take into account athletic performance and longevity in Martial Arts Tricking.

VI: References and Appendices

[1] Pearson, J.N., 1997. Kinematics and Kinetics of the Taekwon-do Turning Kick.

[2] Perez, D.R., 2014. A Kinematic Analysis and Comparison of a Martial Arts Standing Spin Kicks and Jumping Spin Kicks (thesis).

[3] Sørensen H., Zacho M., Simonsen E. B., Dyhre-Poulsen, P., Klausen K. Dynamics of the martial arts high front kick, Journal of Sports Sciences, (1996)14:6, 483-495, DOI: 10.1080/02640419608727735

[4] Ghazirah M, Jamaluddin M, Muzammer Z, Wan Ruzaini Wan S. Biomechanics research on martial arts – the importance of defensive study. Arch Budo 2015; 11: 187-195

[5] Maria Roy Felix J, Ashwin P. Mathematics of Karate Techniques – Dynamics & kinematics of karate. Int J. of Comp. Algorithm 2014; 03: 586-589

[6] Baharuddin M.Y, Hashim A, Sayuti Mohd Salim M. Motion Analysis for Different Type of Jumping. ICADME 2009 (conference)

[7] Mkaoer B, Jemni M, Amara S, Chaabéne H, Tabka Z. Kinematic and Kinetic Analysis of Two Gymnastics Acrobatic Series to Performing the Backward Stretched Somersault. J Hum Kinet. 2013 Jul; 37: 17-26.

[8] Huang C, Hsu G. Biomechanical Analysis of Gymnastic Back Handspring. ISBS 2009 (conference). DOI: 10.13140/2.1.2776.9600

[9] Kadaba MP, Ramakrishnan HK, Wootten ME. Measurement of lower extremity kinematics during level walking. J Orthop Res, 1990 May; 8(3): 383-92

[10] Chomack J, Lombardi N, Schafer R, Gielo-Perczak K. Operators Manual: A Dynamic and Multi-System Approach for Evaluating Leg Injury. University of Connecticut.

[11] Kim JW, Kwon MS, Sushma Yenuga S, Kwon YH. The effects of target distance on pivot hip, trunk, pelvis, and kicking leg kinematics in Taekwondo roundhouse kicks. J Sports Biomech, 2010; 9(2): 98-114

[12] Bradshaw EJ, Hume PA. Biomechanical approaches to identify and quantify injury mechanisms and risk factors in women's artistic gymnastics. J Sports Biomech, 2012; 11(3): 324-341

[13] Mcneal JR, Sands WA, Shultz BB. Muscle activation characteristics of tumbling take-offs. J Sports Biomech, 2007; 6(3): 375-390

[14] Yahia-Cherif L, Gilles B, Molet T, Magnenat-Thalmann N. Motion capture and visualization of the hip joint with Dynamic MRI and optical systems. Comp Anim & Virtual

Worlds 2004; 15(3-4): 377-385

[15] Biomechanics & Physics of Sport. TopendSports. [URL]: http://www.topendsports.com/biomechanics/

[16] Tricking. Awakepedia. [URL]: https://www.awakeningfighters.com/awakepedia/tricking/

[17] Cluett J. Orthopedic Statistics and Demographics – Information about stats and numbers in orthopedic surgery. (2015) [URL]: https://www.verywell.com/orthopedic-statistics-and-demographics-2548685

[18] Davis III RB, Ounpuu S, Tyburski D, Gage JR. A gait analysis data collection and reduction technique. Hum Move Sci 1991; 10(5): 575-587

[19] Borhani M, McGregor AH, Bull AMJ. An alternative technical marker set for the pelvis is more repeatable than the standard pelvic marker set. Gait & Posture 2013; 38(4): 1032-1037

[20] OptiTrack (2017). [URL]: http://optitrack.com/

[21] The Motion Monitor (2017). [URL]: http://www.innsport.com/